UNIVERSITY OF OKLAHOMA

GRADUATE COLLEGE

A 13-YEAR TRAJECTORY-BASED ANALYSIS OF CONVECTION-DRIVEN CHANGES IN UPPER TROPOSPHERE LOWER STRATOSPHERE COMPOSITION OVER THE UNITED STATES

A THESIS

SUBMITTED TO THE GRADUATE FACULTY

in partial fulfillment of the requirements for the

Degree of

MASTER OF SCIENCE IN METEOROLOGY

By

EMILY NICOLE TINNEY
Norman, Oklahoma
2020

A 13-YEAR TRAJECTORY-BASED ANALYSIS OF CONVECTION-DRIVEN CHANGES IN UPPER TROPOSPHERE LOWER STRATOSPHERE COMPOSITION OVER THE UNITED STATES

A THESIS APPROVED FOR THE
SCHOOL OF METEOROLOGY

BY THE COMMITTEE CONSISTING OF

Dr. Cameron Homeyer, Chair

Dr. Naoko Sakaeda

Dr. Steven Cavallo

Acknowledgments

This thesis would not be possible without the brilliance, kindness, and unwavering support of Dr. Cameron Homeyer. I say with entire honesty that I could not imagine a better advisor. The growth that I have experienced as a scientist over the past two and a half years in undoubtedly due his impeccable mentorship. From the first day, Dr. Homeyer made OU and the CCC research group feel like home. He sets the bar so very high, but I hope that one day I will be half the scientist that he is.

This work has also been improved upon and supported by a number of other scientists. I would like to thank Ms. Andrea Gordon for largely informing this study through her sensitivity testing of results to various reanalyses datasets. I would also like to acknowledge Dr. Nathaniel Livesey and Dr. Michael Schwartz of the MLS team at the NASA Jet Propulsion Laboratory, as well as three anonymous reviewers, for their helpful comments and suggestions regarding this work. I would also like to thank Dr. Naoko Sakaeda and Dr. Steven Cavallo for serving on my Master's Committee. I am fortunate and thankful to have learned so much from both of them in their classes.

I of course need to acknowledge my fellow CCC group members, both past and present, for their scientific and emotional support. I would especially like to thank Elisa Murillo and Thea Sandmæl for enormous amounts of help when I was first getting started, and for being amazing women and scientists to look up to. I am also extremely thankful for the extended work family that I have in Office 5700. Though we have not been physically present in the NWC for a while, our office shenanigans are the highlight of my time so far at OU.

Lastly, I am so very thankful to whole family for encouraging me and supporting me as I chase my dreams. I am especially grateful for my mom, Susan Tinney, whose faith in me has never faltered. She is the reason I know what it means to be strong. I am also incredibly thankful for my life partner, Owen Sanchez. From moving across the country with me to proofreading every email I send, he has been there

every step of the way supporting and encouraging me every single day. Finally, my thank-yous would not be complete without acknowledging my two wonderful kitties, Gizmo and Leia. The past 14 years of my life have been blessed by the companionship that I have in Gizmo. He is genuinely the perfect cat; I am not sure how I would've survived the transition to graduate school without him. Leia joined our family within the last year and has us brought so much joy, especially when it comes to her obsession with food.

The most challenging part of completing this work was that much of it occurred in the middle of a global pandemic. I am incredibly thankful for everyone working on the front lines and putting their own health at risk in order to help others. I want to extend a thank you to every person who puts on a mask every time they go in public and to every person who has made personal sacrifices in the name of public health. It is because of the people who put the greater good before themselves that we will one day make it out of this crisis.

This work was supported by the National Aeronautics and Space Administration (NASA) under Award 80NSSC18K0746.

Table of Contents

List of Tables

List of Figures

Abstract

Moist convection frequently reaches the tropopause and alters the distribution and concentration of radiatively important trace gases in the upper troposphere and lower stratosphere (UTLS), but the overall impact of convection on regional and global UTLS composition remains largely unknown. To improve understanding of convection-driven changes in water vapor (H_2O), ozone (O_3), and carbon monoxide (CO) in the UTLS, this study utilizes 13 years of observations of satellite-based trace gas profiles from the Microwave Limb Sounder (MLS) aboard the Aura satellite and convection from the operational network of ground-based weather radars in the United States. Locations with and without convection identified via radar are matched with downstream MLS observations through three-dimensional, kinematic forward trajectories, providing two populations with unprecedented sampling of trace gas observations for analysis. These populations are further classified as belonging to extratropical or tropical environments based on the tropopause pressure at the MLS profile location. Extratropical regions are further separated by tropopause type (single or double), revealing differing impacts. Results show that convection typically moistens the UT by up to 300% and the LS by up to 100%, largely reduces O_3 by up to 40%, and increases CO by up to 50%. Pronounced changes of H_2O and O_3 are found, with LS O_3 reduced more by convection within tropical environments, where the median concentration decrease is 34% at $\sim$2 km above tropopause, compared to 24% in extratropical environments. Quantification of CO changes from convection is less reliable due to differences being near the MLS measurement precision and accuracy.

Chapter 1

Introduction

Moist convection has the ability to facilitate rapid two-way transport of air across the tropopause, a process referred to as stratosphere-troposphere exchange (STE) (Holton et al., 1995). While there are many processes that can facilitate STE, deep convection is the smallest in scale and is arguably the least understood. Convective transport and its associated STE have been observed in aircraft observations in the tropics and extratropics, but its frequency, geographic distribution, vertical extent, and large-scale significance have not been well characterized. Our limited understanding of chemistry, transport, and STE in convection is due, in large part, to limited capabilities of global observing systems and to the limited number of high-resolution case studies of *in situ* measurements in storms (Gettelman et al., 2011). Furthermore, most previous work focuses on upward transport (or troposphere-to-stratosphere transport) in convection and its impact on the upper troposphere and lower stratosphere (UTLS), while recent studies such as Pan et al. (2014), Frey et al. (2015), Homeyer (2015), and Phoenix et al. (2020) indicate that stratosphere-to-troposphere transport can also be extensive in these storms. The troposphere and stratosphere are chemically distinct airmasses, and STE is critically important to the climate system through its impact on the Earth's radiation budget by changing the vertical distribution and concentration of trace gases in the UTLS.

The vertical distribution of water vapor (H_2O) is particularly susceptible to convective influence. H_2O is prevalent in the troposphere while the stratosphere (in the absence of convective influence) is typically very dry, with H_2O mixing ratios around 3–6 ppmv (e.g., Tilmes et al., 2010). When convection overshoots the tropopause, it can inject H_2O into the stratosphere via two pathways: air mass transport and

ice particle detrainment (which subsequently sublimates in the subsaturated environment). H_2O is a powerful greenhouse gas, and Solomon et al. (2010) have shown that a sustained reduction of only 0.5 ppmv in global mean LS H_2O leads to a 25–30% decrease in the rate of decadal surface warming. Estimations of convective contributions to stratospheric H_2O vary widely in the literature, likely related to the various methods implemented to examine this process despite observational limitations. Hanisco et al. (2007) and Dessler and Sherwood (2004) suggest that up to 45% of H_2O in the stratospheric overworld (where $\theta > 380$ K) comes from convective injection, while more recent studies suggest much smaller impacts (e.g., Schoeberl et al., 2018; Ueyama et al., 2018). Additionally, there is some disagreement about the role that convection plays in UTLS hydration in the tropics, as some studies indicate that tropical tropopause-overshooting convection can both hydrate and dehydrate the UT, depending on the humidity of the pre-convective environment (e.g., Jensen et al., 2007; Hassim and Lane, 2010).

Convection can also significantly change the vertical distribution of ozone (O_3) in the UTLS, which is typically low in concentration in the troposphere and high in the stratosphere. O_3 has its greatest radiative forcing in the UT, with concentration increases in the UTLS leading to surface warming (Lacis et al., 1990). In contrast to H_2O, convection impacts the vertical distribution of O_3 in the UTLS primarily through air mass transport. Both observational and modeling studies have shown that convection-driven stratosphere-to-troposphere transport increases O_3 concentration in the UT as O_3-rich stratospheric air is wrapped underneath a storm anvil (Pan et al., 2014; Phoenix et al., 2020). There has additionally been some evidence that convection can increase LS O_3 by mixing higher-O_3 stratospheric air downward near the overshooting top (Frey et al., 2015). Conversely, convectively-driven troposphere-to-stratosphere transport has been shown to decrease LS concentrations of O_3 (e.g., Dessler and Sherwood, 2004; Hegglin et al., 2004). It has been argued that decreases

in stratospheric O_3 may also occur if increases in H_2O from convection are large enough and the temperature is low enough to activate rapid O_3-destruction chemistry (Anderson et al., 2012, 2017; Schwartz et al., 2013). Convective transport of alternative trace gases that are mostly passive, such as carbon monoxide (CO), has also been of interest in previous studies due to their utility as a tracer of boundary layer air (e.g., Jiang et al., 2007).

Satellite- and aircraft-based studies have attempted to distinguish the overall large-scale impact of convection on UTLS composition. Randel et al. (2012) used satellite observations of isotopic composition of H_2O and found that convection occurring over the United States is uniquely capable of injecting copious amounts of ice into the LS. Subsequent work has shown that a region over North America that contains $\sim$1% of Microwave Limb Sounder (MLS) H_2O observations accounts for more than half of observations with concentrations greater than 11 ppmv at 100 hPa (Schwartz et al., 2013). While those extreme values have not been explicitly tied to convective sources, Smith et al. (2017) found that the frequency and location of extreme stratospheric H_2O concentrations are broadly consistent with the seasonal and geographical distribution of tropopause-overshooting convection and Jensen et al. (2020) further showed that convective hydration at 100 hPa and 82.5 hPa within the LS over North America occurs primarily in the summer months during the monsoon season. These previous efforts largely neglect UTLS impacts from convection in low tropopause environments, for which overshooting is more common and extends further into the LS over the contiguous United States (CONUS; Cooney et al., 2018). Although to a lesser extent than H_2O, MLS observations have also been used to investigate convection-related depletion of O_3. Schwartz et al. (2013) showed that in July-August, O_3 concentrations at 100 hPa (82.5 hPa) are $3 \pm 1\%$ ($6 \pm 1\%$) lower in regions that meet thresholds of chlorine activation regimes identified by Anderson et al. (2012) than in similar, drier parcels. However, some proportion of the decreased

O_3 concentrations can likely be attributed to dilution by tropospheric air. The extent to which chemical destruction of O_3 occurs is still largely unknown and is a topic of debate within the community (e.g., Robrecht et al., 2019).

Recent climatological studies of tropopause-overshooting convection do not provide information on its chemical impact, but can be used as an indicator of convection-driven STE frequency. Regardless of region/environment (tropics or extratropics), studies using observations from ground- and satellite-based precipitation radar and cloud lidar show that tropopause-overshooting storms are most frequent over land (e.g., Liu and Zipser, 2005; Pan and Munchak, 2011; Liu and Liu, 2016; Solomon et al., 2016). Tropopause-overshooting convection can occur at any time throughout the year, but there exists a strong annual cycle in occurrence that peaks in the late spring/early summer, especially over land in the midlatitudes (Solomon et al., 2016). In a 10-year analysis of hourly radar data over the United States, Cooney et al. (2018) found an average of more than 44,000 warm season overshooting events each year, though this is likely at least a factor of 4 underestimate due to the hourly sampling interval of the study and typical overshoot lifetimes of 5-15 minutes (Fujita, 1974). The vast majority of overshooting occurs over the central Great Plains, with the monthly geographic distribution of overshoots gradually shifting poleward throughout the warm season. Cooney et al. (2018) additionally showed that nearly half of tropopause-overshooting convection reaches into the stratospheric overworld where residence times of trace gases are longer and therefore convection can have a larger impact on overall composition. The environment in which convection occurs can impact its efficiency in facilitating such deep overshooting and STE. In particular, if a double tropopause (a low-stability layer above the primary tropopause altitude) is present at the location of convection, deeper convective overshooting is common (Homeyer et al., 2014; Solomon et al., 2016).

Various satellite-based identification methods have been developed to study deep convection and the role it plays in STE. For example, Berendes et al. (2008) uses visible and near-IR texture and reflectance to objectively identify overshooting convection, but this method can only be used in the daytime and struggles with low solar zenith angles. Alternatively, Bedka et al. (2010) uses infrared window channel brightness temperature gradients to detect tropopause-overshooting convection. This method can be used both day and night, but it relies on large-scale analysis for temperature profiles and therefore does not account for thermodynamic modification of the environment by convection and has a substantial false-alarm rate (up to 38.8%). Brightness temperatures are used in a number of other methods to infer cloud top heights, but most fail to account for modification of the UTLS by convection and potential mixing between the convective cloud top and the stratosphere. Recent development of multispectral pattern recognition techniques (combining visible and multiple IR imagery) has improved upon some of the limitations of these prior efforts, achieving false alarm rates less than 20% (Bedka and Khlopenkov, 2016). An alternative method of observing overshooting convection from the ground was introduced by Homeyer (2014), which merged observations from multiple ground-based radars into volumes with high resolution in the vertical. This method has since been improved and successfully used in a number of studies (e.g., Homeyer et al., 2014; Homeyer and Kumjian, 2015; Solomon et al., 2016; Cooney et al., 2018).

In summary, it is well-known that deep convection frequently reaches the tropopause (especially over land in the midlatitudes during summer) and impacts the distribution and concentration of chemically and radiatively important trace gases in the UTLS. However, the small-scale, rapid nature of convective transport and responsible dynamical and physical processes remain poorly understood and rarely sampled at fine scales, thus hindering our ability to discern the overall impacts of convection on trace gases in the UTLS. As such, there is a critical need for long-term regional and global

observational studies of convective influence on UTLS composition. In order to improve understanding of the large-scale impact of convection on UTLS composition and to provide an assessment for its representation in simulations of past and future climates, we seek to bridge past efforts using radar observations of convection and satellite observations of composition by employing a trajectory-based matching technique. In particular, this study utilizes observations from 13 years of satellite-based trace gas profiles from the MLS aboard the Aura satellite and ground-based weather radars from the operational Next Generation Weather Radar (NEXRAD) network in the CONUS to quantify the impact of convection on UTLS composition.

Chapter 2

Data

2.1 Radar Data

The NEXRAD network consists of more than 140 Weather Surveillance Radar-1988 Doppler (WSR-88D) systems over CONUS (Crum and Alberty, 1993). WSR-88Ds observe volumes of clouds and precipitation in polar coordinates on a grid defined by azimuth, range, and elevation relative to the radar site. These volumes are obtained every ∼5 minutes when convection is occurring and contain radar reflectively at horizontal polarization Z_{H}, radial velocity V_{R}, and velocity spectrum width σ_{V} at a minimum.

For analysis, we use large-area mergers of the NEXRAD observations known as Gridded NEXRAD WSR-88D Radar (GridRad) data (Bowman and Homeyer, 2017). GridRad data are available hourly from 1995–2017 on a regular 0.02° longitude-latitude and 1-km altitude grid (Homeyer and Bowman, 2017) and include Z_{H} and multiple variables that keep track of the number of single-radar observations merged into the common data volume. As described in Homeyer and Bowman (2017), the GridRad algorithm is a four-dimensional time- and space-weighted binning procedure that merges individual radar data onto one large rectangular domain extending from 115°W to 69°W longitude, 25°N to 49°N latitude, and 1 to 24 km in altitude. Echo top altitudes, the highest point where Z_{H} exceeds a specified threshold, are the primary product used for analysis in this study as they help to indicate the location and intensity (or lack thereof) of deep convection. Prior to identifying the echo top altitudes at each 1-hour GridRad analysis time, quality-control methods are employed as recommended in Homeyer and Bowman (2017), where low-confidence

and infrequently-sampled echoes are removed. This process almost entirely eliminates common sources of error (or artifacts) such as side-lobe contamination and sun strobes.

2.2 Trace Gas Observations

Profiles of trace gases used to determine the influence of convection on the composition of the UTLS in this study are sourced from the Earth Observing System (EOS) MLS v4.2x aboard the Aura satellite. The Aura spacecraft has existed within the NASA Afternoon Constellation of satellites (the A-Train) since its launch in 2004. The constellation follows a sun-synchronous orbital track, with equator-crossing times of 0130 and 1330 Local Time. Quality-control recommendations for the MLS are provided in Livesey et al. (2020), all of which are employed here to prevent inclusion of potentially biased trace gas observations in the analysis.

The instrument measures the concentrations of 16 different trace gases as well as five atmospheric parameters by measuring thermal microwave emissions in five different frequency ranges. The MLS vertically scans the atmospheric limb in the forward direction of orbital motion and takes 240 scans per orbit with a 1.5° great circle along-track separation (∼160 km) between scans (Waters et al., 2006). Retrievals of constituents and additional parameters by the MLS occur at numerous frequencies and altitudes, resulting in unique spatial resolution, precision, and accuracy of the measurements for each observable. Version 4.2x level 2 MLS measurements of H_2O, O_3, CO, and temperature (T) in the UTLS (300-50 hPa) are utilized in this study. H_2O is retrieved at twelve levels per decade of pressure, O_3 at twelve (six) levels per decade at pressures greater (less) than 215 hPa, and CO at six levels per decade. The retrieval interval of temperature varies widely between ∼3–12 levels per decade of pressure in the UTLS. The spatial resolution, precision, accuracy, and retrieval ranges

Table 2.1: MLS v4.2x observation along-track horizontal resolution, vertical resolution, precision, accuracy, and retrieval ranges.

Observation	**Δx (km)**	**Δz (km)**	**Precision**	**Accuracy**	**Retrieval Range**
O_3	300–400	2.5–3.5	20–40 ppbv	20–50 ppbv ± 0–20%	261–0.02 hPa
H_2O	175–200	1.4–3.1	5–40%	6–25%	316–0.002 hPa
CO	450–690	4.9–5.4	14–19 ppbv	20–30 ppbv ± 30%	215–0.0046 hPa
T	165–167	3.7–4.2	± 0.6–0.8 K	-2.5 to 1 K	261–0.001 hPa

of each are provided in Table 2.1. Only MLS profiles within the region confined by 120°W to 60°W and 20°N to 55°N are considered for analysis in this study.

The spatial resolution of the Aura MLS observations (Table 2.1) is coarse with respect to the scales typical of individual storms and associated transport. However, the primary objective of this study is to determine whether or not convection is a significant contributor to changes in UTLS composition over relatively large spatial scales, such that finer spatial resolution than what Aura MLS provides is not required. Past work has shown that while MLS sometimes underestimates the absolute magnitude of extreme H_2O concentrations due to horizontal and vertical averaging, it generally captures extreme features that have been shown in previous flight campaigns (Schwartz et al., 2013; Herman et al., 2017; Smith et al., 2017). A number of studies have employed MLS observations and similar datasets to study regional signatures of convective transport (e.g., Randel et al., 2012; Schwartz et al., 2013; Smith et al., 2017).

2.3 Reanalysis

This study employs both 3-hourly assimilations of the global atmosphere from the Modern-Era Retrospective analysis for Research and Applications, Version 2 (MERRA-2) and 6-hourly assimilations from the interim version of the European

Center for Medium-Range Weather Forecasts Re-Analysis (ERA-Interim). Parameters of interest include the height of the tropopause, the three-dimensional wind field, and additional meteorological variables. In particular, the tropopause altitude is critical for UTLS studies. Tropopause altitudes are computed at the native vertical resolution of each reanalysis using the World Meteorological Organization (WMO) temperature lapse-rate definition (World Meteorological Organization, 1957), which is generally considered to be a good marker of the vertical discontinuities in static stability and composition at the troposphere-stratosphere boundary (e.g., Gettelman et al., 2011). MERRA-2 is available from years 1979-present at a horizontal resolution of $\sim$0.6° longitude-latitude with 72 model levels, and a vertical resolution of $\sim$1100 m in the UTLS (Gelaro et al., 2017). ERA-Interim output is available from 1979–2019 at a horizontal resolution of $\sim$0.75° longitude-latitude with 60 model levels, and a vertical resolution between 750–1250 m in the UTLS (Dee et al., 2011).

Chapter 3

Methods

As outlined in Chapter 1, this study examines a 13-year period of overlapping GridRad and MLS data, from the first full year of MLS observations in 2005 to the last available year of hourly GridRad data in 2017. Analysis is performed across the entire year, but we present composition results here for the warm season (March-August) only, since tropopause-reaching convection is relatively uncommon in the cool season (Solomon et al., 2016). Unless otherwise noted, results by month are consistent with the aggregated results for the entire warm season, which we focus on here to maximize sample size at all altitudes. To analyze convection-driven changes in UTLS composition, convectively impacted UTLS air identified using radar observations is matched with downstream MLS observations through three-dimensional, kinematic forward trajectories driven by 3-hourly MERRA-2 winds in the TRAJ3D trajectory model (Bowman, 1993; Bowman and Carrie, 2002; Bowman et al., 2013). Namely, trajectories are matched with individual MLS layers that are within specified time and distance thresholds. Detailed steps of the trajectory initialization and calculation, MLS matching, and profile analysis are provided below and illustrated in Figure 3.1.

3.1 Step 1 - Trajectory Initialization

To identify regions with and without convection for trajectory initialization, we compute echo top altitudes and pressures every hour during the study period using the GridRad and reanalysis datasets. First, $Z_{\mathrm{H}} = 15$ dBZ echo top altitudes are determined in regions that are well sampled (at least 40 single-radar elevation scans merged into grid volumes within a column, as informed by analyses from Cooney et al. (2018) and Homeyer (2014)) by identifying the maximum altitude where at least three

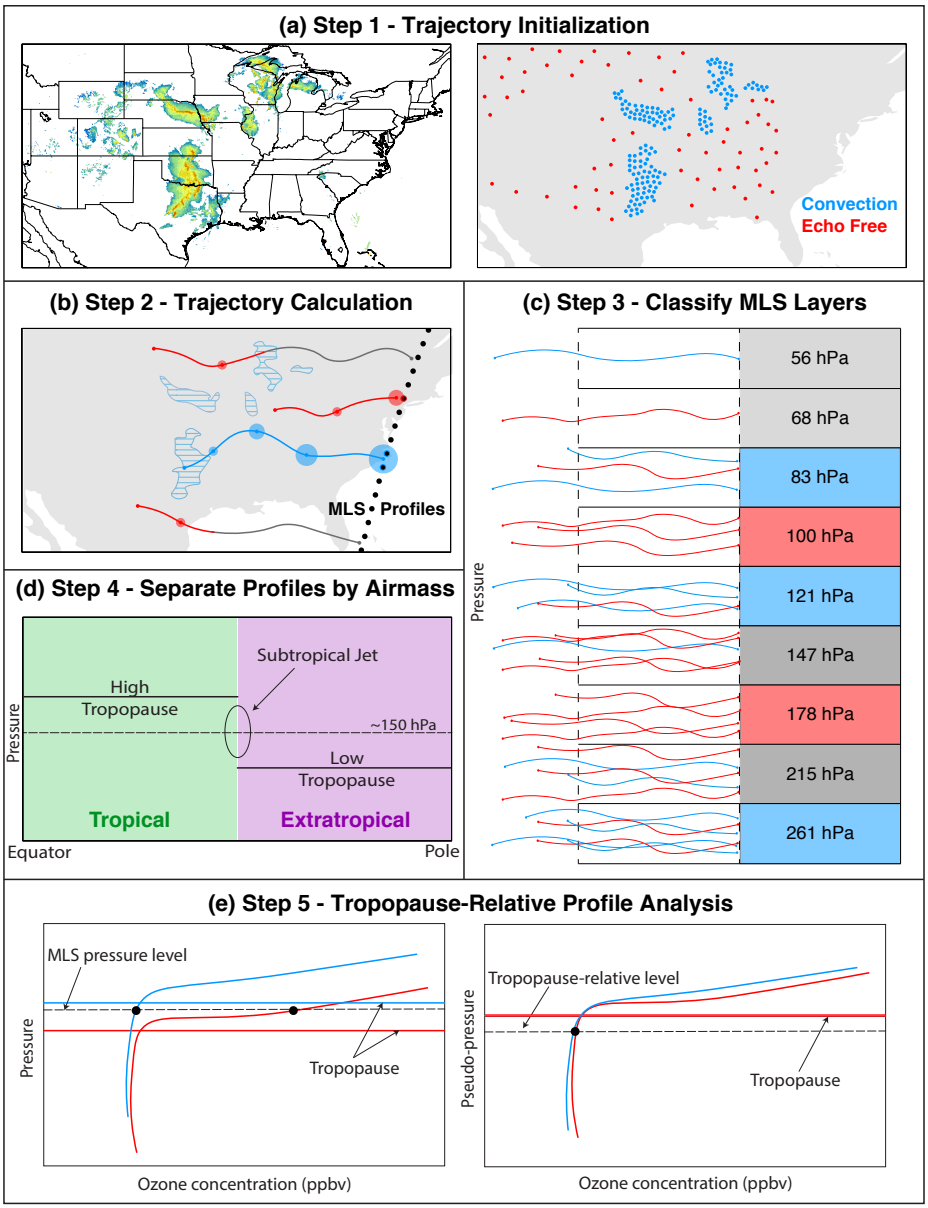

Figure 3.1: A step-by-step illustration of the trajectory initialization and calculation, convection and composition data matching, and analysis procedure used in this study. Trajectory particles and paths corresponding to those initialized in convection and echo-free regions are colored in blue and red throughout, respectively. Blue and red circles in step 2 (panel b) indicate the time-dependent search radius used to account for expected horizontal displacement errors in the trajectory calculations.

consecutive 1-km layers below exceed the Z_{H} threshold (a continuity constraint). The continuity constraint helps to mitigate contamination by spurious echoes that may not be removed by the quality-control procedures. At each grid point, echo top altitudes are then converted to pressures using the geopotential heights and pressures of the nearest reanalysis grid column. Echo top pressures that occur at altitudes above the lowest altitude observed by MLS (pressure of 316.228 hPa) are then identified to initialize convective trajectory particles at the corresponding longitudes, latitudes, and overlapping altitudes between the lowest MLS measurement and echo top (Fig. 3.1a).

For comparison with particles initialized in convection, an additional set of particles is initialized randomly throughout the GridRad domain in well-sampled regions where no echo is found above an altitude of 4 km above sea level (about 50,000 particles per day). These echo-free trajectory particles are placed at every MLS pressure level to facilitate comparison with convective particles.

3.2 Step 2 - Trajectory Calculation

All convective and echo-free trajectory particles are advected forward for three days beyond initialization using the TRAJ3D model and reanalysis wind fields, with positions saved hourly along the trajectory path (Fig. 3.1b). Following trajectory calculation, the echo history along the paths of echo-free trajectories is examined to ensure that these parcels have not been influenced by convection following their initialization. Any echo-free trajectories that pass within a specified time-dependent distance from convection are discarded. This time-dependent search radius R, in km, increases with increasing time since particle initialization, given by:

$$R = 60 \times \frac{h}{24} \tag{3.1}$$

where h is the number of hours elapsed. This approach accounts for expected horizontal displacement errors in the trajectory calculations (60 km day^{-1} here), which are dependent on the spatial and temporal resolution of the input wind fields. A displacement error of 60 km per day is assumed for the reanalysis data used to drive the trajectory model in this study based on prior trajectory sensitivity studies to the spatiotemporal resolution of input wind fields (Stohl et al., 1995; Bowman et al., 2013). All trajectories are additionally required to be well-observed by radar along at least 80% of their paths to be retained for analysis.

3.3 Step 3 - MLS Matching and Classification

Following trajectory initialization and calculation, the resulting particle locations are matched with individual altitude layers within MLS profiles (Fig. 3.1c). This trajectory matching is accomplished by applying a similar time-dependent distance criteria to a potential match, $D = 80 + R$, where the 80-km minimum distance is approximately half of the MLS along-track sampling interval, which is comparable to the along-track horizontal resolution of many of the retrieved quantities (Livesey et al., 2020). Namely, for each MLS profile, the locations of all trajectory particles initialized within the preceding 3-day period are compared to the MLS profile location at the time the profile was retrieved. If a trajectory particle lies within D km of an MLS profile location, it is matched with the layer it overlaps with closest in altitude so long as it falls within the MLS layer depth (in log pressure). It is possible for a trajectory particle to be matched with more than one MLS profile, but we do not allow particles to be matched with more than one layer in a profile.

Following matching with trajectory particles, individual MLS layers are classified as "convective" or "echo-free" based on the number and ratio of the matches. In order to be classified as an echo-free layer for analysis, there must be no convective trajectories matched with that layer. To be classified as a convective layer, at least

50% of the matched trajectories must be convective. Only layers with $\geq$ 50 total trajectory particle matches are analyzed in order to limit the analysis to layers where there is a confident understanding of their recent history.

MLS layers that are determined to belong to an extratropical air mass (described in Section 3.4) are further separated and classified by whether there was a single tropopause (ST) or double tropopause (DT) present at the location of trajectory initialization, as tropopause type can impact both background trace gas composition and the overshooting depth of convection (Homeyer et al., 2014; Schwartz et al., 2015; Solomon et al., 2016). For a layer classified as convective, if more than two thirds of the convective trajectories were initialized in a DT environment, then it is classified as a DT layer. For a comparison population, echo-free layers are also classified as DT layers if more than two thirds of the matched echo-free trajectories were initialized in a DT environment. Similarly, to be classified as a ST profile, more than two thirds of the matched convective or echo-free trajectories must have been initialized in a ST environment.

3.4 Step 4 - Profile Separation by Air Mass

Matched MLS profile layers are classified as belonging to tropical or extratropical air masses based on the altitude of the tropopause at the MLS profile location (Fig. 3.1d). There exists a sharp discontinuity in the height of the lapse-rate tropopause near the subtropical jet that is commonly referred to as the "tropopause break", which enables the tropopause pressure itself to be a suitable and commonly implemented approach to delineate between extratropical and tropical environments (e.g., Randel et al., 2007; Homeyer and Bowman, 2013; Boothe and Homeyer, 2017). Therefore, we classify MLS layers in this study as extratropical where the pressure of the tropopause is $>$ 150 hPa ($\leq\sim$15 km altitude) and tropical where the tropopause pressure is $\leq$ 150 hPa ($>\sim$15 km altitude).

Geographic distributions for extratropical and tropical convective and echo-free warm season matches are shown in Figure 3.2. As expected, tropical matches are commonly located in the southern half of the domain and extratropical matches in the northern half, though both populations can be found across most of the domain since the corresponding environments meander north and south with the subtropical jet stream. Differences between the locations of convective and echo-free matches within each environment are largely longitudinal. Namely, convective matches in extratropical environments are found at slightly greater distances off of the east coast, likely due to predominately eastward advection by the subtropical jet. For tropical environments, convective matches are found more often in the southeast United States (where there is frequent convection in summer) and echo-free matches are found more often in the southern Great Plains (commonly within the interior of the North American monsoon anticyclone, where there is infrequent convection).

3.5 Step 5 - Tropopause-Relative Profile Analysis

To develop an adequate and reliable understanding of the impacts of STE on UTLS composition, a well-utilized approach to analysis is to collect observations in tropopause-relative altitude coordinates (Pan et al., 2004; Tilmes et al., 2010; Gettelman et al., 2011). Tropopause-relative altitude coordinates help to preserve sharp discontinuities in composition that exist and enable identification and evaluation of the extent of STE above and below the tropopause. Thus, we conduct our analysis of MLS layers in tropopause-relative space to enable reliable evaluation of convective influence on UTLS composition (Fig. 3.1e). Tropopause heights used at the location of the MLS profiles are sourced from the reanalyses. Trajectory-matched MLS layers are placed into tropopause-relative logarithmic pressure (originally in hPa) bins. We use two different bin resolutions to account for the differing vertical resolutions of each variable by MLS. H_2O, O_3, and temperature (CO) observations are placed into

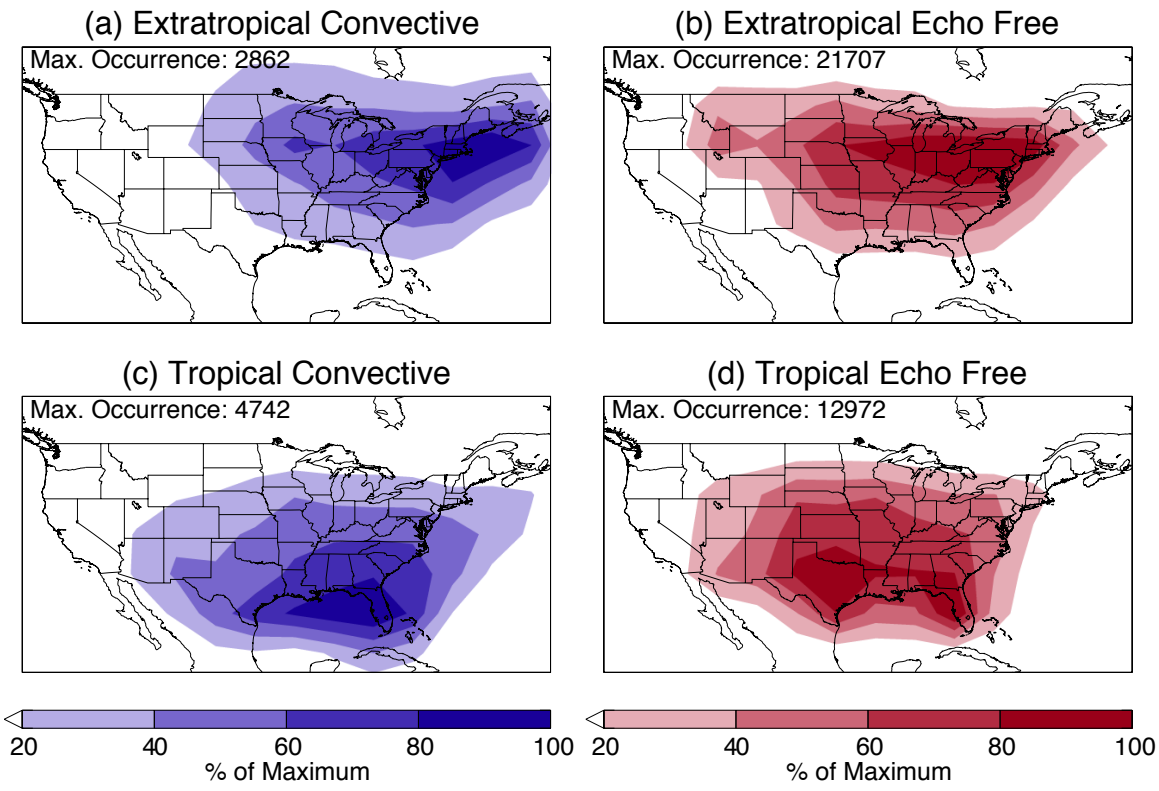

Figure 3.2: Normalized geographic distributions of MLS observations matched with (left) convective and (right) echo-free trajectories in both (top) extratropical and (bottom) tropical environments. Match locations are binned on a 5° latitude-longitude grid, with the maximum occurrence of matches in any bin (used for normalization) displayed in the top left corner of each panel.

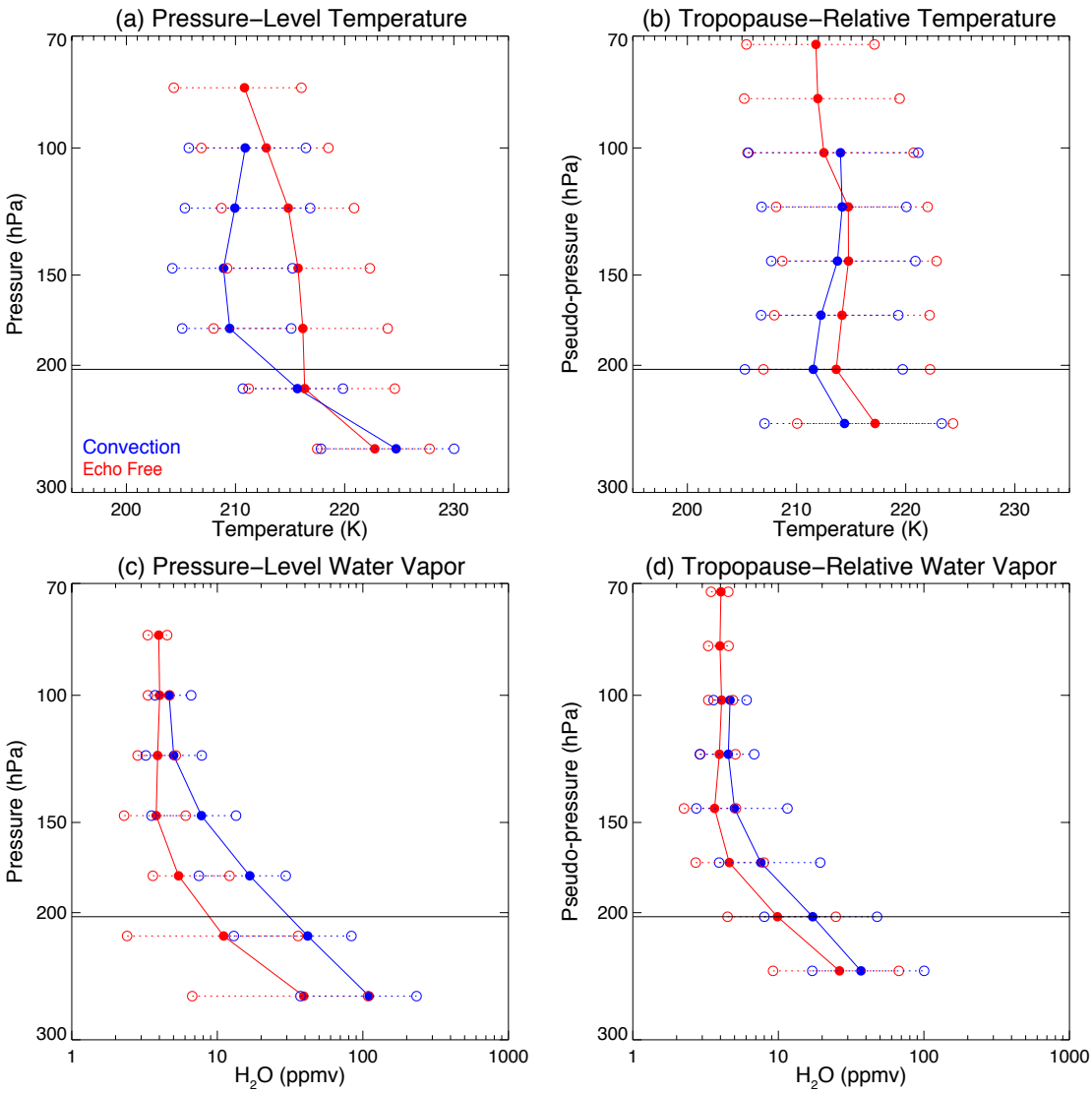

Figure 3.3: For MLS observations within extratropical environments only: pseudo-profiles of trajectory-matched convection (blue) and echo-free (red) layers (left) at native pressures and (right) in tropopause-relative pressure layers for (top) temperature and (bottom) water vapor. For each pseudo-profile, filled circles and solid lines indicate median values as a function of pressure, while open circles and dashed lines indicate the 10th to 90th percentile range of values at each level. Horizontal solid lines in each panel indicate the average altitude of the tropopause for all trajectory-matched layers analyzed, sourced from ERA-Interim in this example.

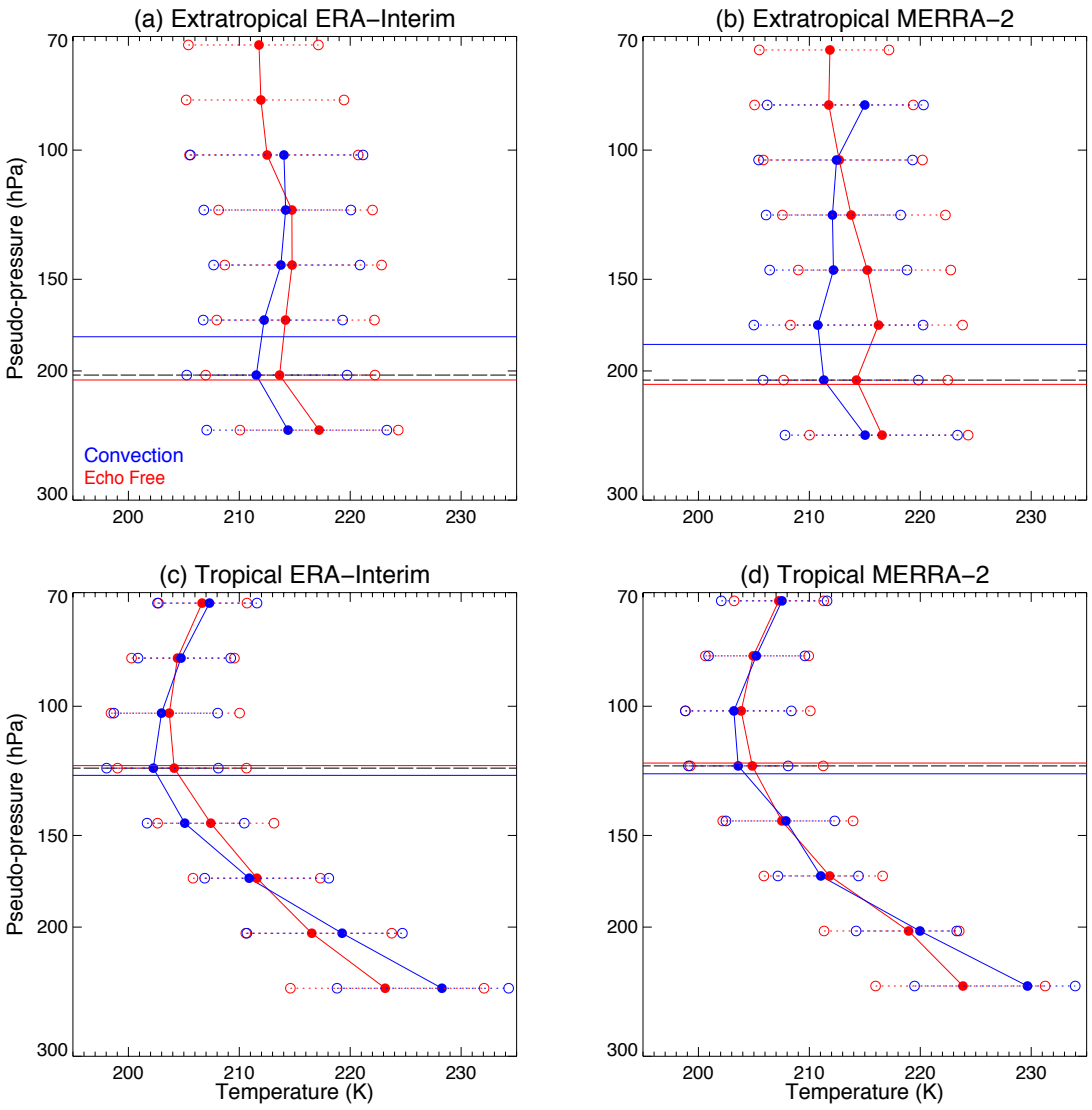

Figure 3.4: As in Fig. 3.3, but for MLS observations of temperature within (top) extratropical and (bottom) tropical environments and in relative altitude to (left) the ERA-Interim tropopause, and (right) the MERRA-2 tropopause. Horizontal dashed lines in each panel indicate the average altitude of the tropopause for all trajectory-matched layers, while solid blue (red) lines in each panel indicate average tropopause altitude of convective (echo-free) trajectory-matched layers only.

bins with a resolution of 0.075 (0.10) decades of pressure, hereafter referred to as "fine resolution" ("coarse resolution") bins. For context, the 0.075 resolution roughly translates to ∼1-km altitude increments in the UTLS for an isothermal atmosphere via the barometric equation. Once binned, the median concentration, 10th percentile, and 90th percentile values of the four variables are computed for all convective and echo-free MLS layers to evaluate distributions of each observable. This is done separately for the extratropical and tropical MLS profiles, as well as the extratropical ST and DT profiles. The tropopause-relative logarithmic pressure bins are then transformed back into a pressure space to create pseudo-profiles for analysis. Only layers with ≥ 100 matched observations are analyzed.

To demonstrate why a tropopause-relative method is preferred, analyses of temperature and H_2O performed both at native MLS pressure levels and in tropopause-relative pressure bins are shown in Figure 3.3. The pressure level analysis of temperature in Figure 3.3a shows large differences between the median convective and echo-free profiles. The average tropopause height from all observations is shown near 200 hPa, but the minimum near-tropopause temperature of the echo-free profile indicates the average tropopause of this population is closer to 215 hPa whereas the average tropopause of convective profiles occurs between 178 and 147 hPa. Thus, at a given pressure greater than ∼150 hPa, many of the MLS layers matched with convection are within the UT while similar layers matched with echo-free regions are often within the LS. Figure 3.3c displays how large of an impact this can have on apparent H_2O differences between the two populations. Median convective H_2O concentrations are much larger than the echo-free concentrations throughout the profile. While some convective moistening is expected, a large component of the differences shown is likely a result of comparing a very dry LS from echo-free layers to a moist UT from convective layers. Thus, it is impossible to isolate the impact of convection on the UTLS in native pressure coordinates. When the analysis is performed in a tropopause-relative

coordinate, the differences between echo-free and convective profiles of temperature and H_2O better reveal the expected impact of convection on the UTLS found in prior case studies. In Figure 3.3b, a tropopause-relative temperature analysis results in a local temperature minimum consistent with the tropopause altitude that is aligned between convective and echo-free populations, with a lower tropopause temperature in convectively influenced air. This tropopause temperature difference is expected given previous findings of convective lifting and cooling of the tropopause in extratropical environments (Homeyer et al., 2014; Maddox and Mullendore, 2018; Starzec et al., 2020).

One important requirement for tropopause-relative analysis is an accurately identified tropopause. Temperature analyses for both extratropical and tropical air masses relative to the ERA-Interim tropopause and the MERRA-2 tropopause are shown in Figure 3.4. The pseudo-profiles are similar in their overall shape, but do have some key differences. In Figure 3.4a, the extratropical ERA-Interim-based temperature profile shows a local minimum occurs at the level of the tropopause with a weak inversion in the LS. In Figure 3.4b, however, the MERRA-2-based convective profile has its lowest temperature one layer above the tropopause and LS inversions have different character than those diagnosed using ERA-Interim. The inconsistencies between MLS retrieved temperature minima and tropopause altitude in the MERRA-2-based profiles likely reflect known biases in tropopause altitude in MERRA-2. Recently, Xian and Homeyer (2019) have shown that the MERRA-2 tropopause is often biased $\sim$100 m high and has a slightly higher (100-200 m) uncertainty than ERA-Interim in the midlatitudes. ERA-Interim has an unbiased tropopause with an uncertainty of $\sim$600 m, which would have a minimal effect on the analysis as it is well below the vertical resolution of MLS observations near the tropopause. For these reasons, our tropopause-relative analysis is conducted using the ERA-Interim tropopause. Note that a sensitivity study of the analysis to the wind field used for trajectory calculation

(MERRA-2 or ERA-Interim) was also carried out, but the results were insensitive to this choice.

Chapter 4

Results

4.1 Bulk composition differences

The number of MLS observations classified as extratropical or tropical for both fine- and coarse-resolution variables at each tropopause-relative altitude are shown in Figure 4.1. Both convective and echo-free air is well sampled in the extratropical and tropical UT, with more than 10,000 (5,000) extratropical (tropical) observations of each. Sampling of echo-free air increases in the LS, while the number of convective layers decreases rapidly, reflecting the increasing rarity of convection reaching heights well into the stratosphere.

Extratropical and tropical psuedo-profiles of temperature (Figs. 3.4a & 3.4c) and H_2O concentrations (Fig. 4.2) are largely consistent with previous work and provide confidence that the trajectory-matched MLS method of analysis is working. As outlined in Section 3.5, local temperature minima occur at the altitude of the tropopause for all populations and convective temperatures are lower at the tropopause and throughout much of the UTLS in both tropical and extratropical environments. While pseudo-profiles are created based on average tropopause height of all trajectory-matched layers, Figure 3.4a shows the average extratropical tropopause associated with convective layers is higher than the average tropopause from echo-free layers and Figure 3.4c shows that the average tropical convective tropopause is actually slightly lower than the echo-free tropopause. Tropical convective temperatures are warmer at the bottom of the profiles, but become lower than echo-free temperatures closer to the tropopause due to increased lapse rates. The convectively influenced temperature profile is consistent with previous work that has shown that deep convective clouds are associated with cold anomalies at the cloud top (near the tropopause) and

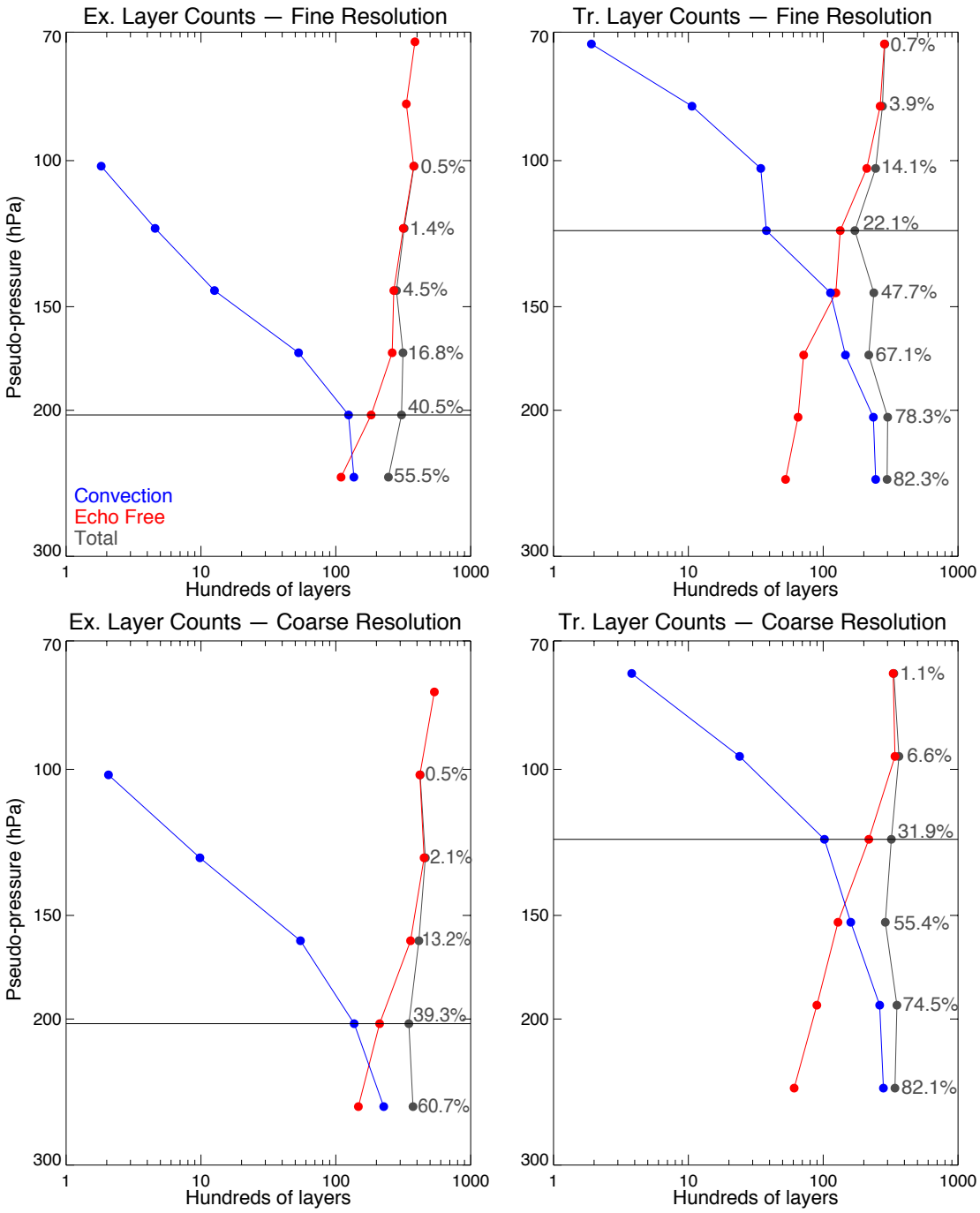

Figure 4.1: As in Fig. 3.3, but for the number of MLS layers analyzed for (top) fine resolution and (bottom) coarse resolution variables within (left) extratropical and (right) tropical environments. The gray line indicates the total number of observations (both convection and echo-free). Numbers along the gray line indicate the percentage of total layers matched with convection at each level.

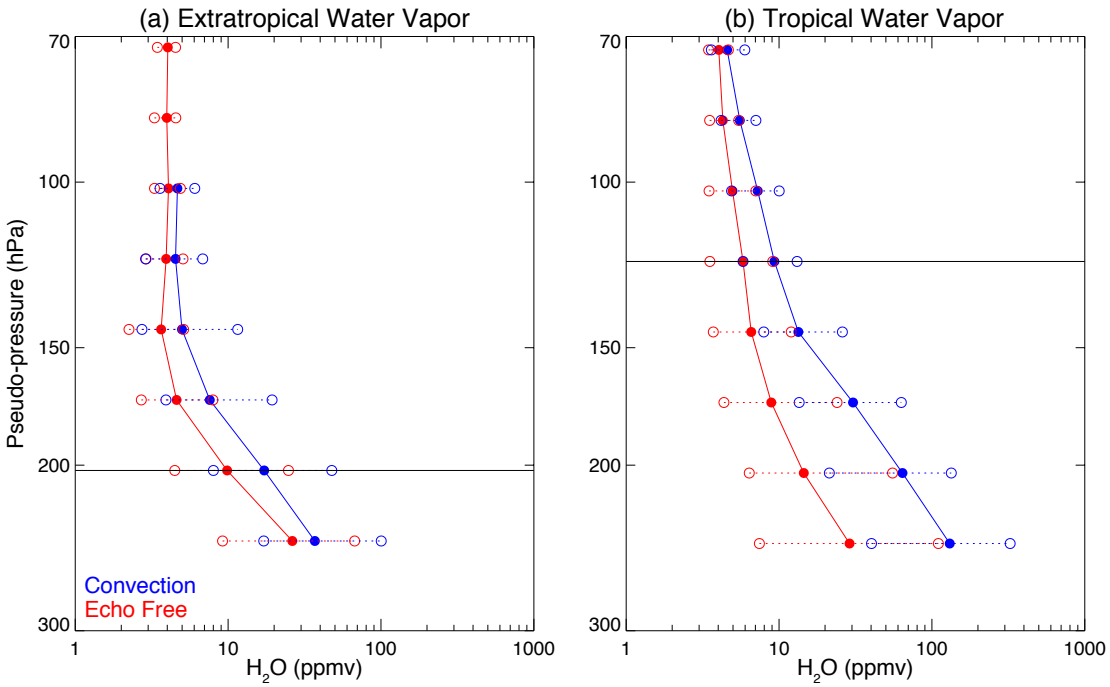

Figure 4.2: As in Fig. 3.3, but for MLS observations of water vapor within (left) extratropical and (right) tropical environments.

increased lapse rates below that often approach a moist adiabatic lapse rate and can result in a lowered tropopause (See Figure 10 in Biondi et al., 2012).

As anticipated, the influence of convection on UTLS H_2O is to moisten the layer (Figs. 4.2a, 4.2b), regardless of bulk differences in environments and tropopause temperature. The entire distribution of the convective observations is shifted to the right of the echo-free observations, with an extratropical median convective H_2O concentration of 18 ppmv and an echo-free concentration of 10 ppmv at the height of the tropopause. In the lowest layer of the LS, the echo-free median is $\sim$4.75 ppmv while the convective median is 8.75 ppmv. Additionally, the distributions of convectively influenced extratropical H_2O reach higher values throughout the UTLS, with 90th percentile concentrations more than doubling the median values throughout much of the profile and the median profile approximately coincident with the 90th percentile echo-free profile throughout the LS. Tropical H_2O concentrations are also strongly

enhanced by convection in the UTLS, especially in the UT. At the lowest UT level, the median echo-free concentration is ∼30 ppmv, while the convective median is ∼150 ppmv. Strong convective moistening persists throughout the UTLS, with median convective concentrations in the LS more than double the median of and at or above the 90th percentile concentration of the echo-free profile. In the LS, convective H_2O concentrations exceed echo-free concentrations by 1–2 ppmv. The 90th percentile concentrations of tropical LS distributions are found at lower concentrations than those in extratropical environments, likely constrained by low saturation vapor concentrations associated with the colder UTLS environments.

Pseudo-profiles of O_3 and CO concentrations are shown in Figure 4.3. In both extratropical and tropical environments, convective O_3 concentrations are smaller than echo-free concentrations at the tropopause and throughout the LS (Figs. 4.3a, 4.3b). Median extratropical convectively-influenced O_3 concentrations are nearly 100 ppbv lower than echo-free concentrations throughout much of the LS, while observations in tropical environments show greater differences (up to ∼200 ppbv lower than echo-free). The decreases in O_3 throughout the LS from convection are also found to reach lower concentrations within tropical environments. Differences in CO concentrations between the convective and echo-free profiles are less apparent throughout most of the LS, with the largest differences (increases) occurring in the UT. In Figure 4.3d, there is a peak in convective CO concentration two levels below the tropopause that may represent the level of maximum detrainment (LMD; Mullendore et al., 2009) for tropical convection. The tropopause-relative level where this peak occurs is ∼3 km below the tropopause. Starzec et al. (2020) found that the LMD occurs between 4 and 5 km below the tropopause in the southern United States in May and July. Our study is based on the full warm season and is not fixed in geographic location, which could explain why this CO peak is observed higher in the UT. The coarse vertical resolution of CO observations by the MLS and limited extent of observations into

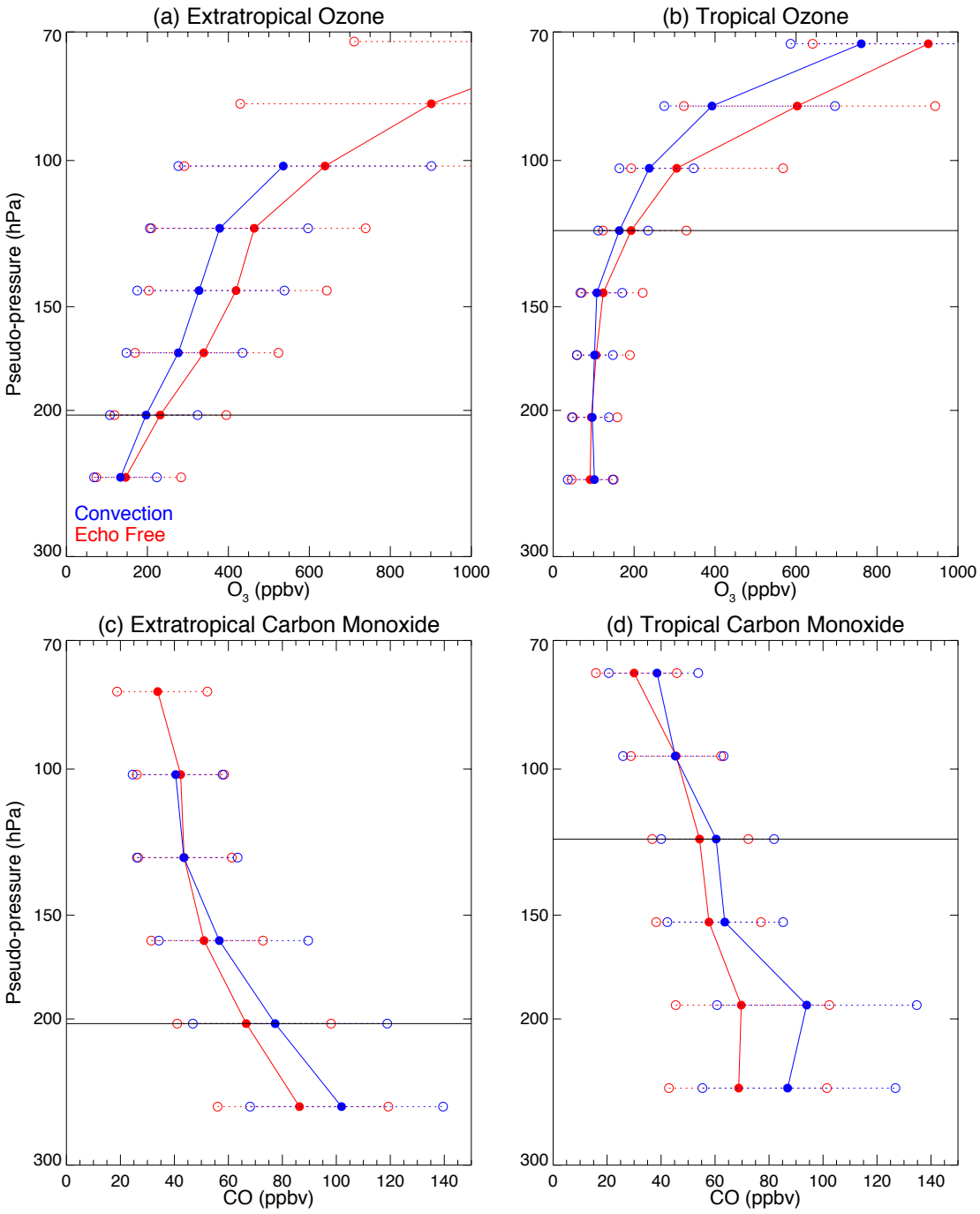

Figure 4.3: As in Fig. 3.3, but for MLS observations of (top) ozone and (bottom) carbon monoxide within (left) extratropical and (right) tropical environments.

the UT could also be influencing the estimated height of this peak. A peak in CO concentration representing the LMD may exist in the extratropical profile as well, but since the tropopause exists at a higher pressure (lower altitude) the MLS is not capable of observing far enough into the troposphere to confirm this. In the LS, the convective influence on CO in both the extratropical and tropical profiles diminishes as concentrations approach the precision and accuracy limits of MLS CO retrieval (see Table 2.1).

4.2 Sensitivities of composition impacts to midlatitude tropopause environment

In extratropical environments, poleward transport associated with rossby wave-breaking events (as well as other processes) can lead to the formation of a DT, where a high tropical tropopause overlaps with a lower extratropical tropopause (e.g., Homeyer et al., 2011). The existence of a DT at the location of convection can have significant implications on the background LS trace gas structure as well as the depth of tropopause-overshooting convection (Homeyer et al., 2014; Schwartz et al., 2015; Solomon et al., 2016). For this reason, extratropical MLS layers are further classified as ST or DT profiles based on the environment where trajectories were initialized as described in Section 3.3. Figure 4.4 shows the number of echo-free and convective observations in ST and DT environments for both fine-resolution and coarse-resolution variables. Sampling of ST environments is comparable to the total extratropical environments shown in Figure 4.1, while DT sampling of both echo-free and convective layers is comparitively low. For fine-resolution variables at the level of the tropopause, there are ∼20,000 total ST layers, but only ∼7,000 total DT layers. As in Figure 4.1, convective sampling decreases rapidly in the LS, with only two LS layers achieving

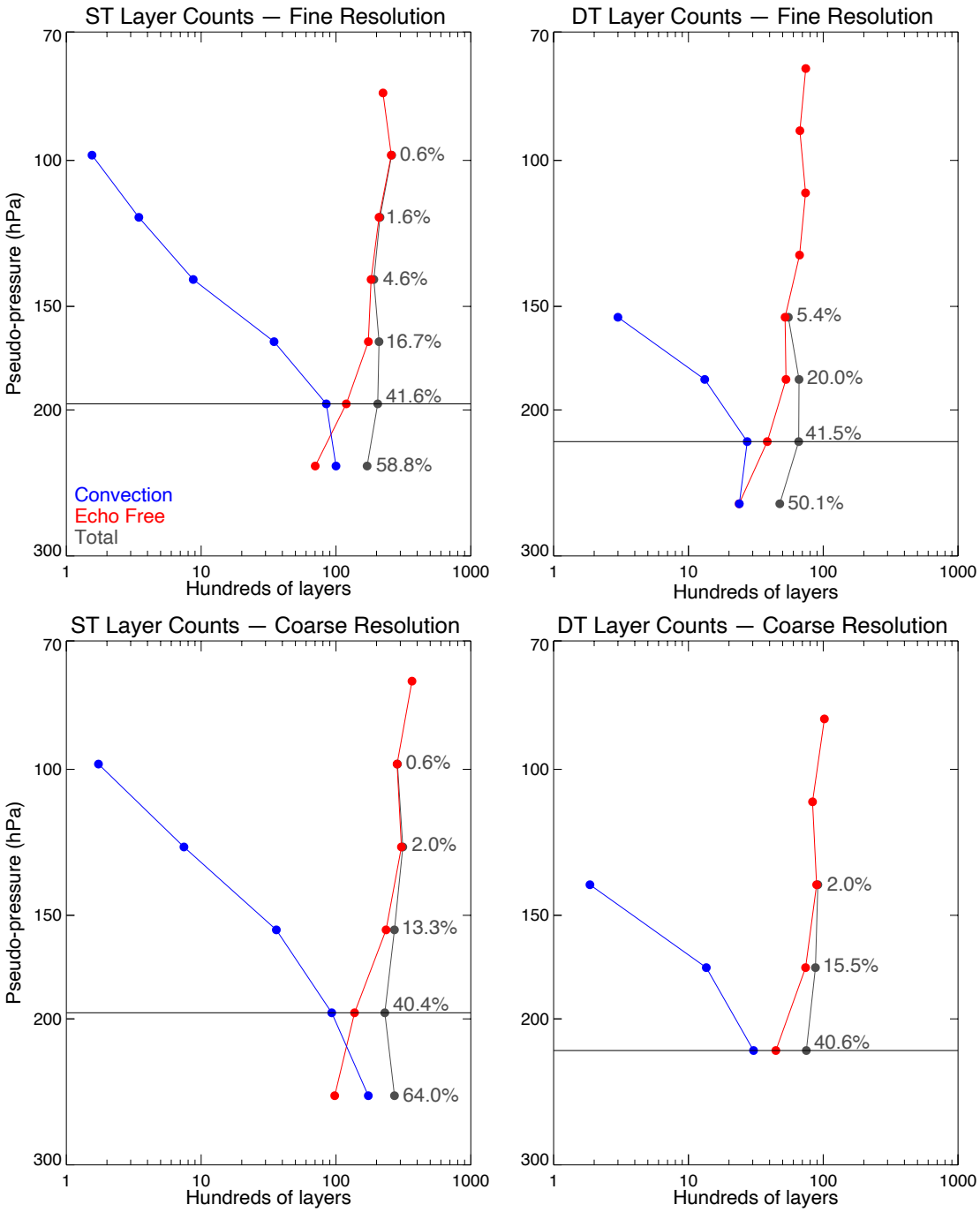

Figure 4.4: As in Fig. 4.1, but for (left) single tropopause extratropical environments and (right) double tropopause extratropical environments.

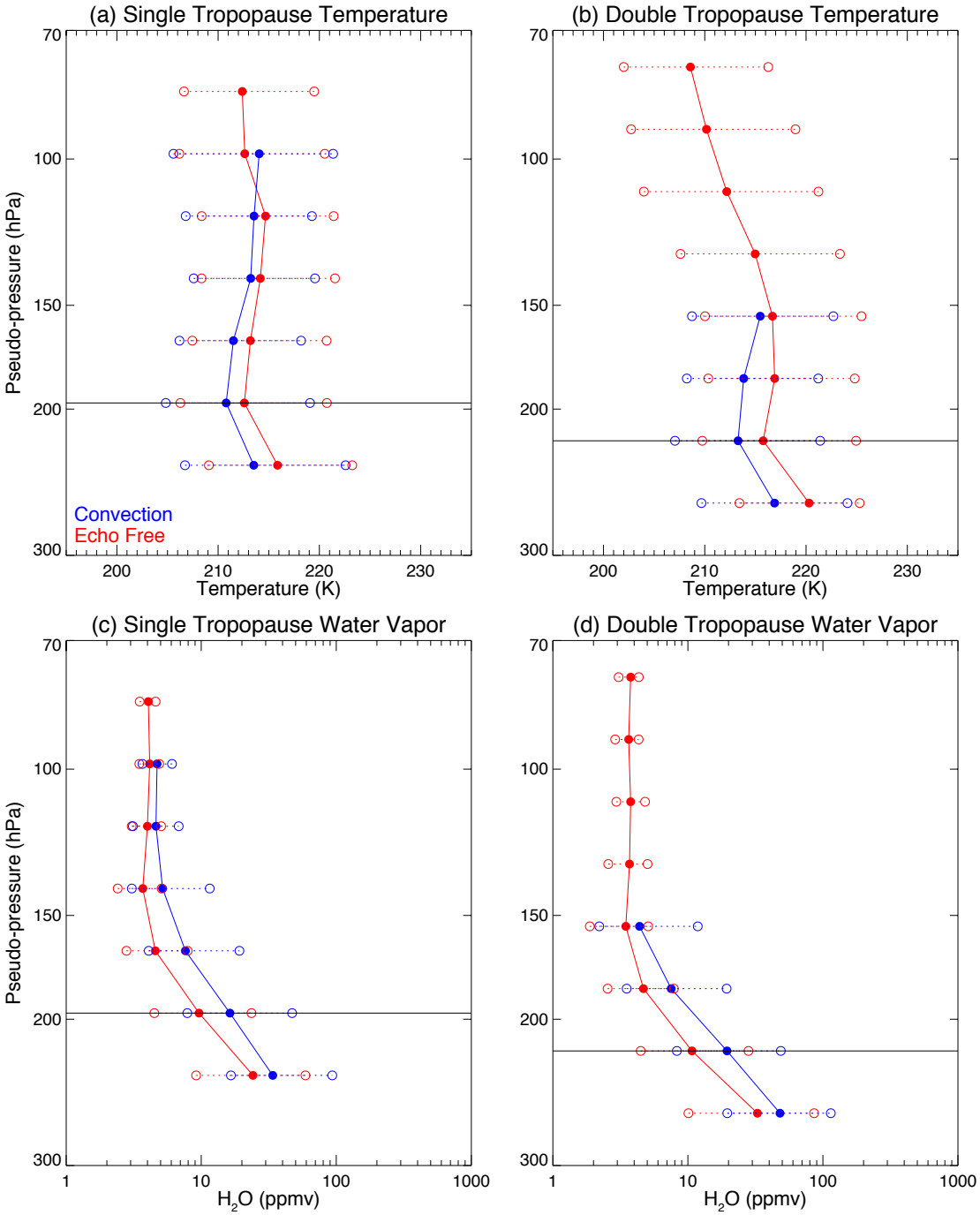

Figure 4.5: As in Fig. 3.3, but for MLS observations of (top) temperature and (bottom) water vapor within (left) single tropopause extratropical environments and (right) double tropopause extratropical environments.

$\geq$100 observations in DT environments. While this sampling is sufficient for meaningful analysis of DT environments, it is important to contextualize the discussion with this sampling in mind given that a wide variety of transport outcomes are possible.

Temperature and H_2O pseudo-profiles for both ST and DT environments are shown in Figure 4.5. The primary (lowest) tropopause in the DT environment is lower in altitude than that in ST environments, at pressures of $\sim$225 hPa and $\sim$197 hPa, respectively, resulting in the temperature at the DT primary tropopause being warmer than that of the ST. Convective temperature decreases are stronger in the DT profile, indicating that convection occurring in a DT environment may displace the tropopause upwards more than in a ST environment or alternatively that the troposphere in non-convective DT environments is typically colder than that in ST environments. The H_2O concentrations are similar between the ST and DT profiles. This is somewhat unexpected, as convection within DT environments typically reaches farther into the stratosphere due to lower stratospheric stability and could arguably result in higher H_2O concentration increases than that common in a ST environment. It is possible that higher concentrations of H_2O occur at higher tropopause-relative altitude than two levels above the tropopause in the DT convective profile and can not be seen in our analysis due to limited sample size, but this seems unlikely. It seems more plausible that the full distribution of changes within a DT environment is not entirely captured by limited sampling (recall Figure 4.4).

ST and DT pseudo-profiles of convective and echo-free O_3 and CO concentrations are shown in Figure 4.6. ST convective O_3 concentrations are smaller than echo-free concentrations throughout the LS, with the magnitudes of the differences exceeding those in the bulk extratropical profiles in Figure 4.3a. In the DT profiles, however, convective O_3 concentrations are effectively indistinguishable from the echo-free concentrations as they fall well within the precision and accuracy limits of the measurement. The ST and DT convective median concentrations of O_3 are similar at

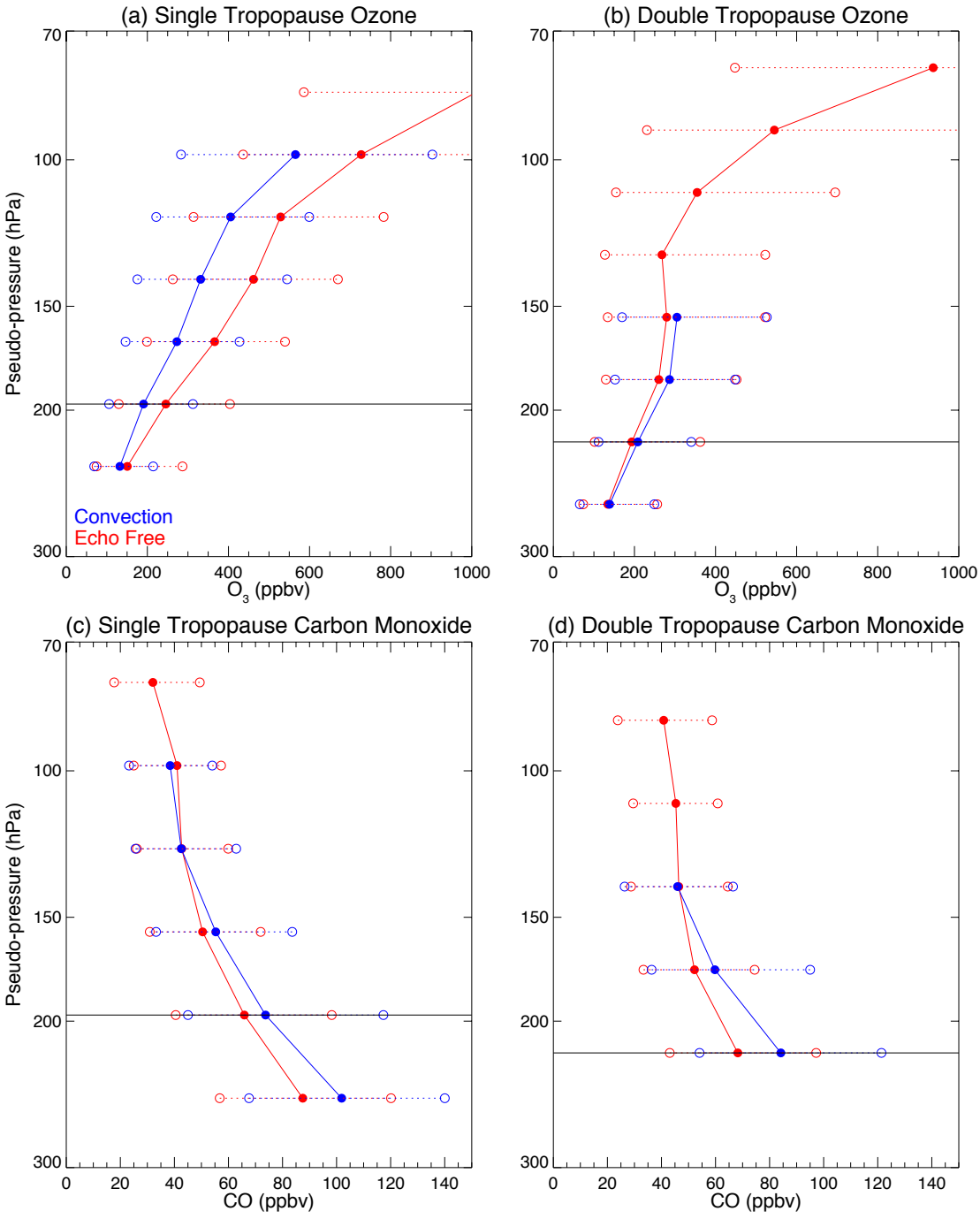

Figure 4.6: As in Fig. 4.3, but for (left) single tropopause extratropical environments and (right) double tropopause extratropical environments.

each tropopause relative level (∼200 ppbv), but the echo-free values in the DT profile are smaller than the echo-free values at the corresponding levels in the ST profile (∼200 and ∼250 ppbv, respectively). Farther above the tropopause, the ST echo-free O_3 concentrations increase while DT concentrations remain low, likely because DT environments are commonly driven by poleward transport of low-O_3 tropical UT air into the extratropical LS (e.g., Pan et al., 2009). In Figures 4.6c and 4.6d, convection in DT environments appears to result in greater increases in tropopause-level and LS CO than in ST environments, though the differences are somewhat small (up to ∼16 ppbv compared to ∼8 ppbv, respectively). The increased concentration of stratospheric CO in the DT profile suggests that storms transport tropospheric air to the UTLS more efficiently when there is a DT present. This is supported by previous work that has shown that DTs allow storms to penetrate higher into the stratosphere and detrain more lower troposphere air near the tropopause (Homeyer et al., 2014; Solomon et al., 2016).

Convection-driven changes in H_2O and CO concentrations are somewhat unexpected and contradictory, with tropopause type making little difference in the convective-influence on H_2O concentrations, while CO concentrations see larger convective increases in DT environments. Considering the sampling results in Figure 4.4, tropopause-level fractions of total trajectory matches associated with convection are nearly equal in ST and DT environments for both fine- (41.6% and 41.5%, respectively) and coarse-resolution (40.4% and 40.6%, respectively) variables. Alternatively, in the first two above-tropopause layers of the LS, convection accounts for a larger fraction of trajectory matches in DT environments than ST environments. This is especially pronounced in the first layer above the tropopause, where the convective percentage of fine-resolution (coarse-resolution) ST observations is 16.7% (13.3%), while for DT observations it is 20.0% (15.5%). This shows that although convection reaches the tropopause at similar rates in ST and DT environments, convection

reaches into the stratosphere at higher rates in the presence of a DT, which is consistent with previous work. While this may partly be a result of the primary tropopause in DT environments being lower in altitude than STs and thus easier for convection to reach, the similar rates of convection reaching the tropopause suggest that decreased stability in the UTLS is a contributing factor. However, this difference does not explain why there are minimal differences in H_2O concentration changes from convection in ST versus DT environments and measurable differences in CO concentration changes. Once again, limited sampling of DT environments could be playing a large role. Another possibility is that CO concentrations are sensitive to the height of the primary (or only) tropopause. As the tropopause is higher in ST environments, high-CO air originating from the boundary layer may be more diluted by the time it reaches the tropopause, thus making increases appear more pronounced in DT environments.

4.3 Seasonally-adjusted composition differences

The results presented thus far are based on a bulk analysis of the Northern Hemisphere warm season. Using a 6-month period for analysis is beneficial due to the large number of profiles available. However, examining the full season allows for seasonality to influence results and makes it difficult to distinguish what composition changes are due to convection directly, and what may be partially influenced by background changes in trace gas concentration. In addition to seasonal changes in trace gases, the average tropopause height changes throughout the year which can also impact the tropopause-relative concentrations of trace gases. The fractions of MLS layers that are classified as convective or echo-free are not constant throughout the year which further allows seasonality to impact results. In order to mitigate these issues, an additional analysis technique is used here to evaluate composition differences relative to

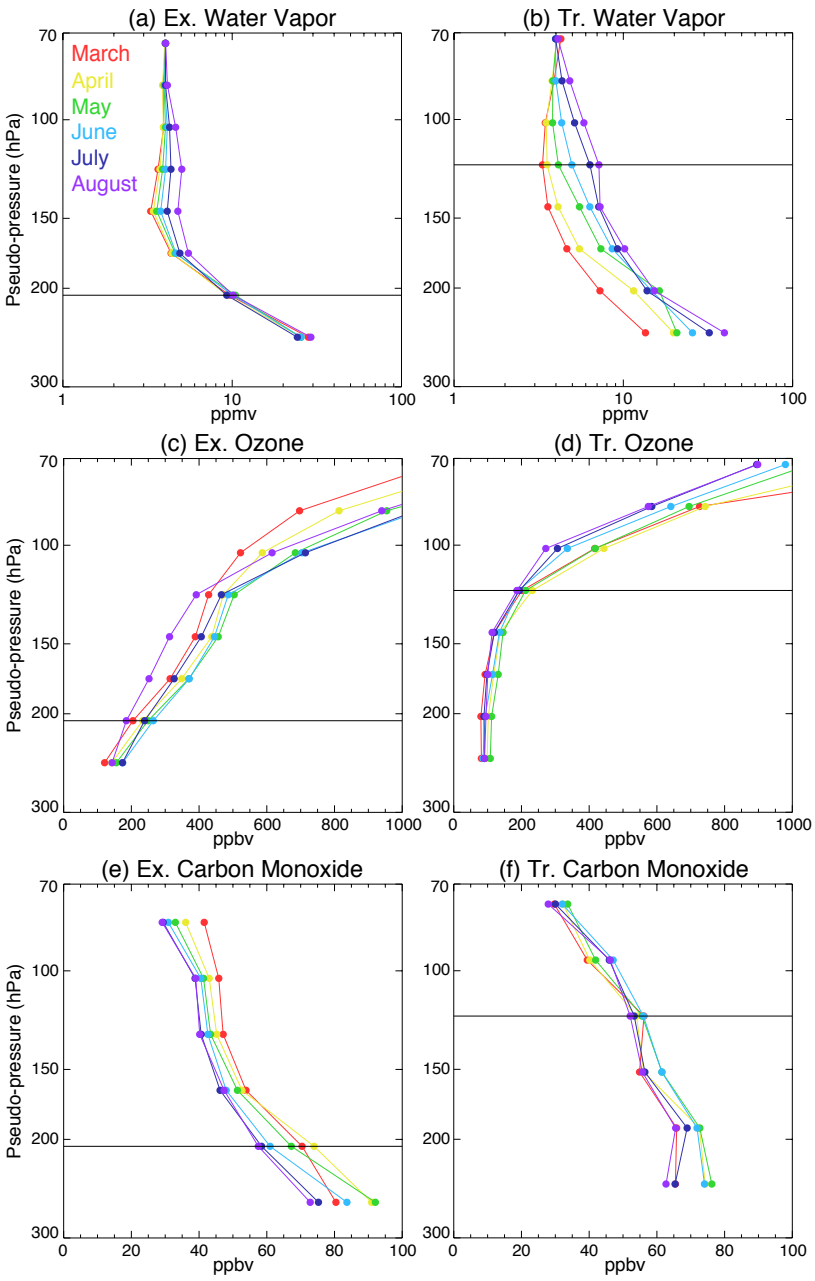

Figure 4.7: Pseudo-profiles of trajectory-matched echo-free layers in tropopause-relative coordinates for monthly median concentrations of (top) water vapor, (middle) ozone, and (bottom) carbon monoxide in (left) extratropical and (right) tropical environments for months March-August. Horizontal solid lines in each panel indicate the average altitude of the tropopause for all trajectory-matched layers analyzed.

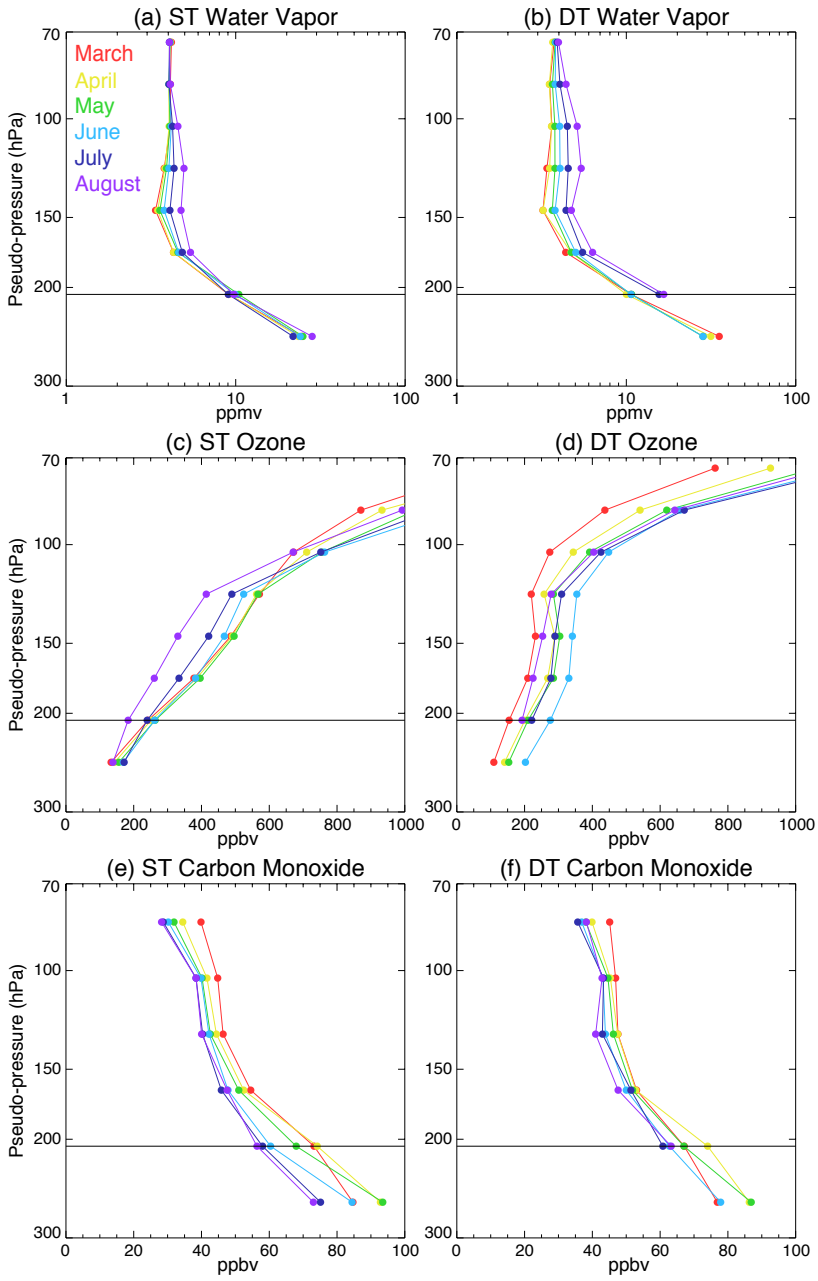

Figure 4.8: As in Fig. 4.7, but for (left) single tropopause extratropical environments and (right) double tropopause extratropical environments.

a seasonally varying background (i.e., echo-free) profile. To do this, the median echo-free concentration of each trace gas is computed at every tropopause-relative level for each month and environment classification (Figs. 4.7 and 4.8). These monthly median profiles are then subtracted from every corresponding convective measurement to compute the de-seasonalized convective anomaly for each trace gas. Every tenth percentile value of these anomalies is then computed for the whole season at each tropopause-relative level to reveal the seasonally-adjusted variability of convective influence.

Given the substantial seasonal changes in trace-gas composition of the UTLS, it is beneficial to approach the seasonally-adjusted convective influence analysis from a relative convective-anomaly perspective rather than absolute differences. These accumulated relative difference distributions for extratropical and tropical H_2O concentration changes are shown in Figures 4.9a and 4.9b, where (as previously indicated in the bulk analysis in Fig. 4.2) convective moistening can be seen throughout the entirety of the profiles. In the 30th to 70th percentile range, extratropical convective moistening is between 20–150% at the level of the tropopause, and 10–100% in the LS. Tropical moistening is extreme in the UT (190–530% in the 30th to 70th percentile range), though this diminishes rapidly closer to the tropopause. The tropical LS typically sees convective increases from 20–60% which is notably smaller than corresponding extratropical LS values. Extreme values in the tropical LS are considerably smaller than in extratropical environments, with values rarely reaching 100% while extratropical LS extremes often exceed 200% increases. This lack of large tropical extremes is likely linked to low tropopause temperatures.

Extratropical and tropical changes in O_3 concentration are shown in Figure 4.10 and are largely consistent with the bulk analysis shown in Figures 4.3a and 4.3b. Throughout the entirety of the profile, extratropical median O_3 concentrations decrease by $\sim$20% when influenced by convection. In the LS, at least 70% of convective

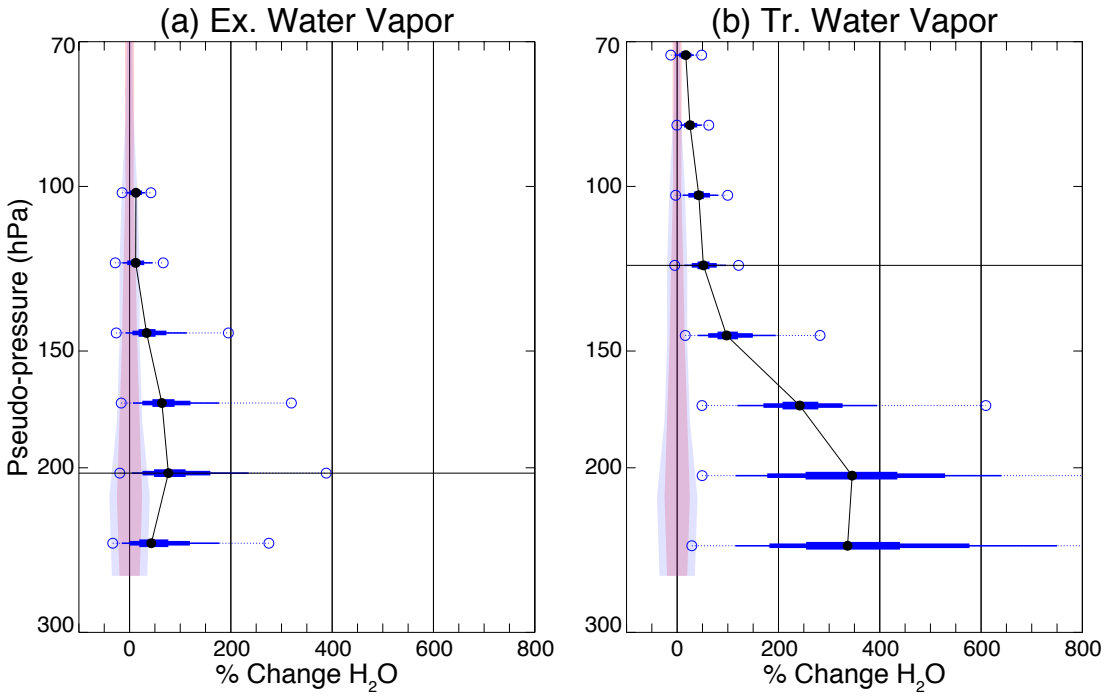

Figure 4.9: Seasonally-adjusted convective anomalies expressed as accumulated relative differences from the corresponding monthly echo-free median concentration of water vapor in (left) extratropical and (right) tropical environments. For each pseudo-profile, filled circles and solid lines indicate median relative difference as a function of pressure, while the horizontal lines from thickest to thinnest represent the 40th to 60th, 30th to 70th, and 20th to 80th percentile ranges, respectively, and the open circles and dashed lines indicate the 10th to 90th percentile range of values at each level. Horizontal solid lines in each panel indicate the average altitude of the tropopause for all trajectory-matched layers analyzed. The average precision of the MLS measurement is shaded in blue and accuracy is shaded in red.

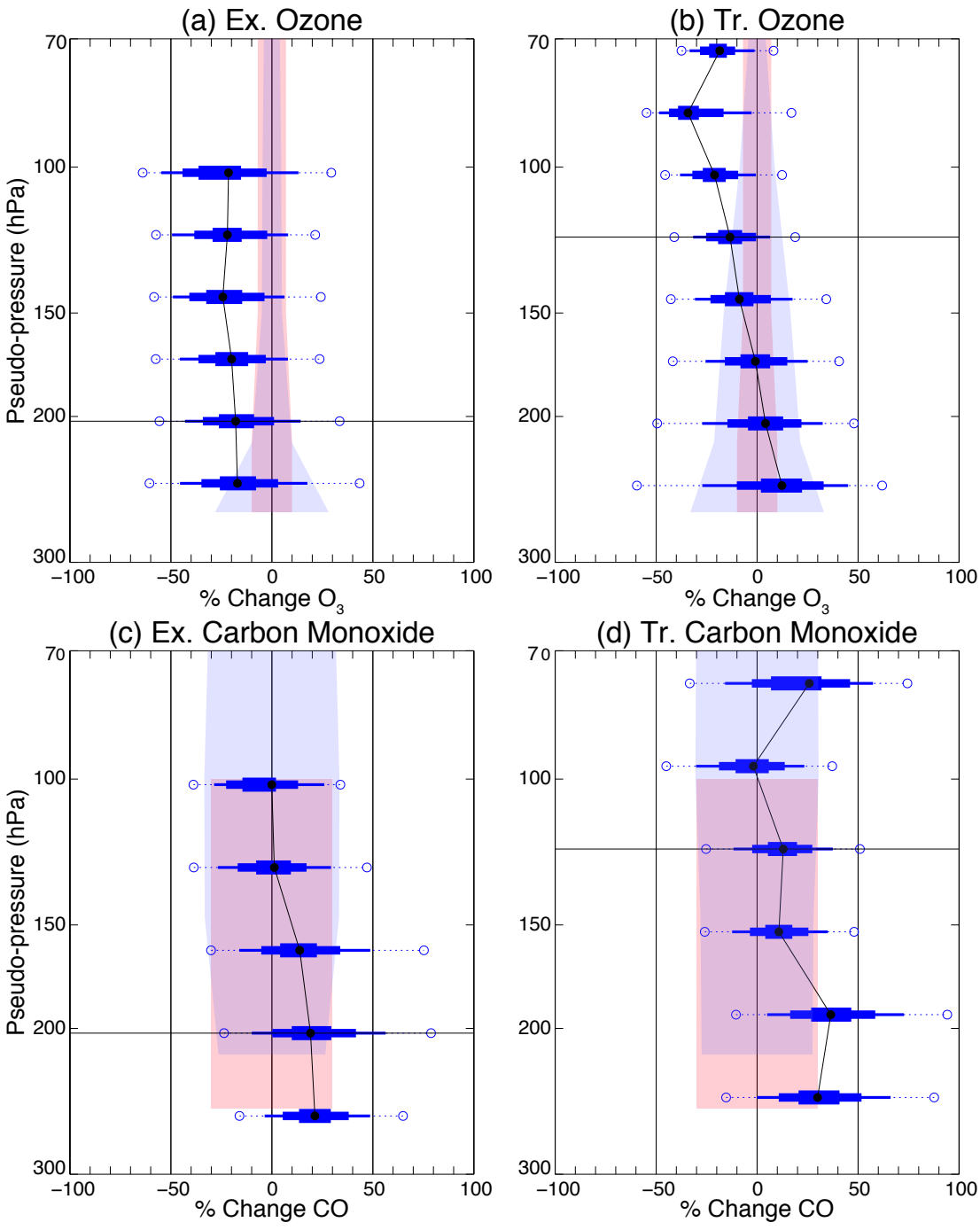

Figure 4.10: As in Figure 4.9, but for (top) ozone and (bottom) carbon monoxide.

profiles contain smaller O_3 concentrations than the echo-free median, with differences commonly reaching −40%. These decreases are likely a reflection of troposphere-to-stratosphere convective transport and mixing of low O_3 UT air into the LS. Tropical changes in O_3 concentration vary with altitude throughout the UTLS. Observational limitations from MLS precision and accuracy are prominent in the tropical UT and inhibit our ability to diagnose convective impact on O_3 with confidence in this region. In the lowest layers of the UT, the median percent change (∼13%) and majority of the difference distribution is positive but falls within the measurement uncertainty. However, more than 30% of profiles exceed these limitations with O_3 increases of more than 22–32%. In the tropical LS, convective decreases in O_3 concentration are seen with the largest decrease (−34% median) found two levels above the tropopause. The median O_3 decrease at this tropopause-relative level in the tropical LS exceeds any median decrease in the extratropical LS (−24%). While some of this tropical O_3 reduction is a result of convective mixing, the larger magnitude of the LS decrease is potentially indicative of chlorine activation and O_3 destruction taking place in the colder tropical environment. This will be further discussed in Chapter 5.

CO changes in extratropical and tropical environments are shown in Figures 4.10c and 4.10d, though limitations from MLS precision and accuracy almost entirely limit confident identification of convective influence. Extratropical CO is convectively increased in the UT and in the lower part of the LS, with 30–40% of profiles showing CO increases that exceed the measurement uncertainty (∼30%). At the two highest levels, convective influence on CO concentration is indiscernible. Tropical convective CO changes are mostly positive but again are mostly confined to values within the MLS precision and accuracy ranges. The only median change that exceeds these uncertainties occurs in the UT at a value of 36%. This occurs at the same level as the CO peak in Figure 4.3d, which as mentioned previously may be indicative of the LMD for convection in tropical environments. Convective influence on CO concentrations

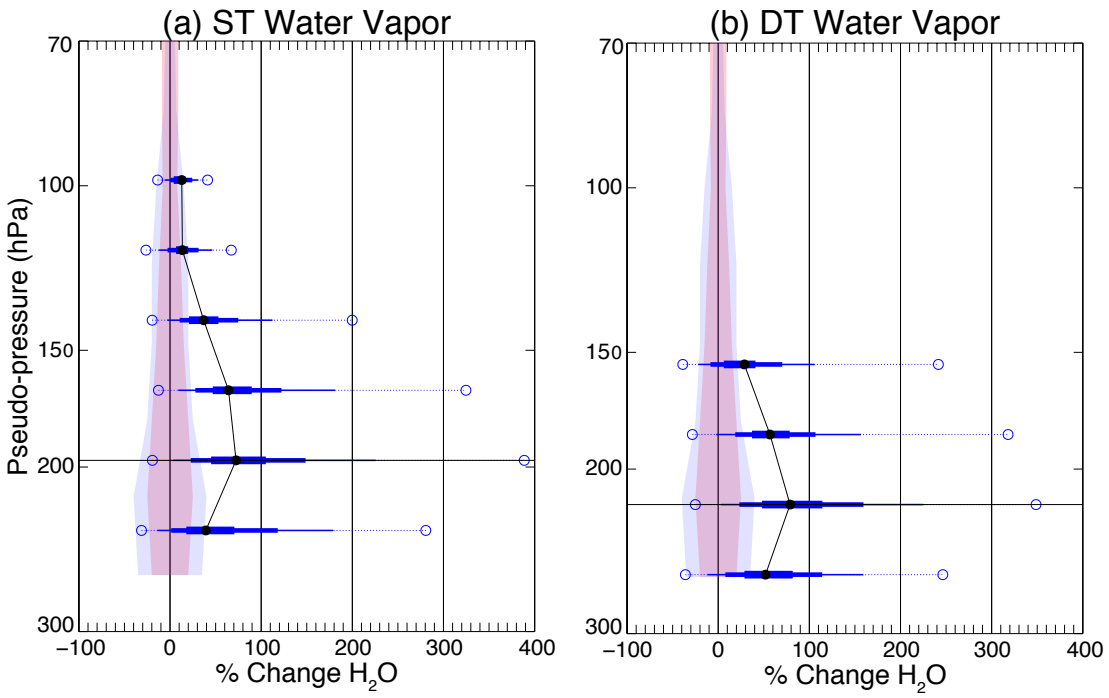

Figure 4.11: As in Fig. 4.9, but for (left) single tropopause extratropical environments and (right) double tropopause extratropical environments.

near the tropopause is less prevalent in tropical environments than extratropical environments, with less than 30% of the difference distribution exceeding uncertainty values. However, at the top level of the tropical pseudo-profile there is a shift in the entire distribution towards higher values where nearly half of the distribution exceeds the precision and uncertainty of the measurement. It is important to note that only 380 convective MLS measurements are sampled at this level while all other levels use at least one order of magnitude more MLS observations (Fig. 4.1d). It is therefore unclear if there is a physical or dynamical reason for this increase or if it is an artifact of reduced sampling at this level.

Seasonally-adjusted difference profiles for the ST and DT breakdown of the extratropical H_2O, O_3, and CO are shown in Figures 4.11 and 4.12. It is clear that tropopause type has little impact on the H_2O changes induced by convection in the

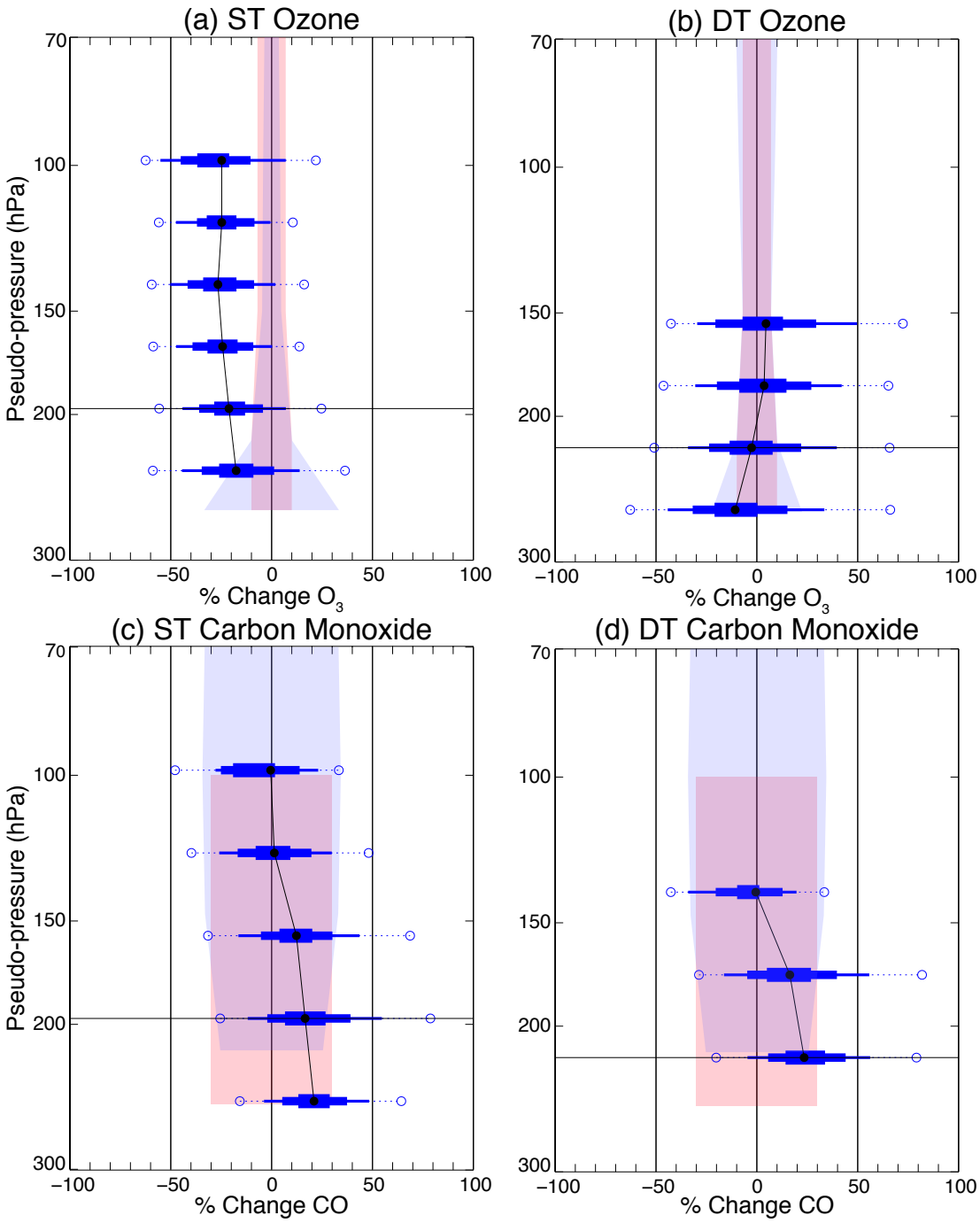

Figure 4.12: As in Fig. 4.10, but for (left) single tropopause extratropical environments and (right) double tropopause extratropical environments.

UTLS, as previously found in the bulk pseudo-profile analysis. Similarly, the differences in convective influence on O_3 and CO within ST and DT environments are in agreement with the bulk analysis, revealing little change in LS O_3 in DT environments and slightly larger increases in CO at tropopause level in DT environments compared to that in ST environments (median differences of $\sim$25% and $\sim$20%, respectively).

Chapter 5

Discussion of LS O_3 Impacts

The overall convection-driven reduction in stratospheric O_3 concentration and its differing magnitude between extratropical and tropical environments is one of the more interesting results identified in this study and warrants further investigation into the processes responsible. We therefore speculate on the importance of some potentially responsible processes by using a simple two-layer linear mixing model to define the expected losses of O_3 due to transport and mixing of tropospheric air into the LS. The model is comprised of a LS layer that is representative of the non-convective background two layers ($\sim$2 km) above the tropopause (where the observed maximum O_3 decrease occurs) and a layer representative of typical O_3 composition within the troposphere. Beginning with the extratropical case, the starting concentration of the LS layer is set to 425 ppbv based on the echo-free analysis (Fig. 4.3a). The starting UT O_3 concentration is set to 75 ppbv, which is notably lower than the observed 150 ppbv echo-free concentration in Figure 4.3a. This concentration was chosen based on climatological studies of tropospheric ozone concentration that show typical values in the range 50–100 ppbv, and because the expected mixing occurs with air originating in the troposphere that has been delivered to the UTLS by convection (Gettelman et al., 2011; Tilmes et al., 2010). Using these concentrations for the two layers, we then solve for the percentage of air in the LS that must be delivered by convection to achieve the observed 24% decrease shown in Figure 4.10a. The resulting estimate of tropospheric air fraction is 29%. Repeating this process for a tropical environment using the same tropospheric O_3 concentration and a LS concentration of 600 ppbv based on the echo-free profile in Figure 4.3b results in a tropospheric air fraction of 39% to achieve the observed decrease of 34% shown in Figure 4.10b. Therefore,

a simple mixing model suggests that 10% more UT air must be mixed into the LS in tropical environments than in extratropical environments to achieve the observed differences in O_3 reduction via mixing alone.

Note that despite the very simple and prescribed approach here, these estimates and the difference between tropical and extratropical fractions are largely insensitive to the endpoint concentrations used. In particular, varying the tropospheric endpoint from 50 to 150 ppb or the stratospheric endpoint ±150 ppbv from the concentrations prescribed leads to a most a ±3% difference from our baseline estimates. Thus, even if the end points differed considerably from those used here or between tropical and extratropical environments, they would still not explain the ∼10% difference observed. Given this limited sensitivity, we considered four possible scenarios that would yield the tropical-extratropical difference: 1) convection in tropical, high tropopause altitude environments is deeper and more vigorous than convection in extratropical, low tropopause altitude environments, 2) background stratospheric concentrations of echo-free environments are not representative of stratospheric concentrations in pre-convective environments, 3) misidentification of the secondary tropopause in an extratropical DT environment as a tropical tropopause alters the concentration of tropical O_3, and 4) air mass mixing in tropical environments is similar to (or weaker than) that in extratropical environments, but there is an additional process (or processes) responsible for the increased ozone reduction in tropical environments (e.g., chemical destruction of O_3).

The first possibility, that storms in high-tropopause environments are deeper and instigate more vigorous mixing is not supported by previous work, such as Cooney et al. (2018) which found that there are few overshoots deeper than 1 km in regions with an average tropopause height greater than 15.5 km (comparable to the 150 hPa tropopause pressure threshold used here to delineate between environments). The second scenario, that convection detrains into a substantially different O_3 environment

than the echo-free background, would introduce non-negligible error in our simple model. However, this situation also seems unlikely given that the echo-free and convective populations are subject to the same spatial and temporal restrictions in this study and that we have additionally verified that the geographic distributions of MLS matches are consistent between the convective and echo-free populations (Fig. 3.2). The third possibility, that tropopause misidentification can influence trace gas concentrations in tropical environments, would require that such misidentifications are more common in one population (i.e., convective or echo-free) and the precise nature of the impact would depend on the favored population. Previous studies have shown that misidentification of a secondary tropopause in extratropical environments as the primary tropopause in model analyses/reanalyses occurs 5-10% of the time over the CONUS (Homeyer et al., 2010; Solomon et al., 2016). By examining Figure 4.8d, it appears that the secondary tropopause likely occurs around ∼125 hPa where the vertical gradient of O_3 increases rapidly, and that this layer (three levels above the primary extratropical tropopause) would be mistaken for a tropical tropopause. In such cases, LS O_3 would appear to be in the UT and could bias these observations in tropical environments. However, this appears to have little impact on diagnosed composition changes at higher altitudes in the LS (where two levels above the tropical tropopause would correspond to five levels above the extratropical tropopause), as the background O_3 concentrations at this level are similar between tropical and DT environments. Therefore, it seems unlikely that tropopause misidentification would have a significant impact on tropical LS O_3 concentrations as the impacts of this seem confined to lower altitudes.

The final scenario, that other processes are contributing to O_3 reduction in tropical environments, seems most likely. Previous studies have identified the possibility of chemical destruction of O_3 through chlorine activation when an airmass is cold and wet enough and contains a sufficient amount of inorganic chlorine, though the

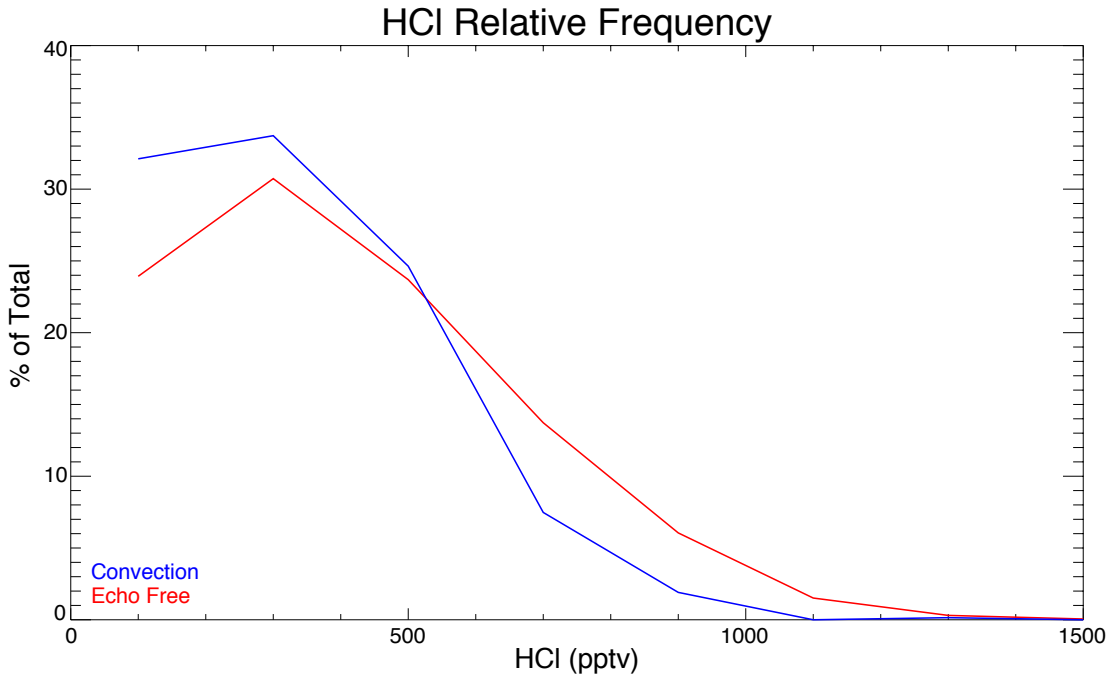

Figure 5.1: A histogram of the relative frequency of HCl concentrations occurring two fine-resolution layers above the tropopause in tropical environments, with a bin size of 200 pptv.

extent of possible destruction is still a subject of debate (Anderson et al., 2012, 2017; Schwartz et al., 2013; Robrecht et al., 2019; Schoeberl et al., 2020). At the level of maximum O_3 reduction observed in convectively-influenced MLS layers within tropical environments, temperatures are less than 205 K ∼50% of the time and less than 200 K ∼10% of the time while H_2O concentrations are typically ∼5–7 ppmv (Figs. 3.4c, 4.2b). MLS observations of hydrogen chloride (HCl) in this same layer reveal a typical background concentration that exceeds 400 pptv ∼45% of the time (Fig. 5.1). Based on these observations and the temperature-H_2O thresholds given in Anderson et al. (2012, 2017) for such O_3 depletion, it is possible that chemical destruction is a contributor to the enhanced LS O_3 decrease within convectively-influenced tropical environments found here. This hypothesis is further supported by the reduction of convective HCl concentrations (shown as a shift in the relative distribution towards lower values than echo-free observations in Figure 5.1), which would occur as HCl is removed during the process of chlorine activation and subsequent O_3 destruction. If we again use our simple two-layer linear mixing model and set the amount of mixing in tropical environments equal to the estimated mixing in extratropical environments (29% tropospheric air), comparable mixing would account for only a 25% decrease in O_3 concentration, leaving 9% of the observed decrease unexplained by mixing. Thus, O_3 destruction from high-H_2O chlorine activation may be responsible for a reduction of up to ∼10% in tropical environments, though definitive attribution of this difference to any particular source is impossible in this study. While this estimate is based on a very simple model that makes a few key assumptions, the model is largely insensitive to its prescribed endpoints and it demonstrates that differences between extratropical and tropical background concentrations alone do not account for the greater reduction in LS O_3 observed in tropical environments.

Finally, to provide broader context for the frequency of convective influence on UTLS air over the CONUS, we show the ratio of all trajectory-matched MLS layers

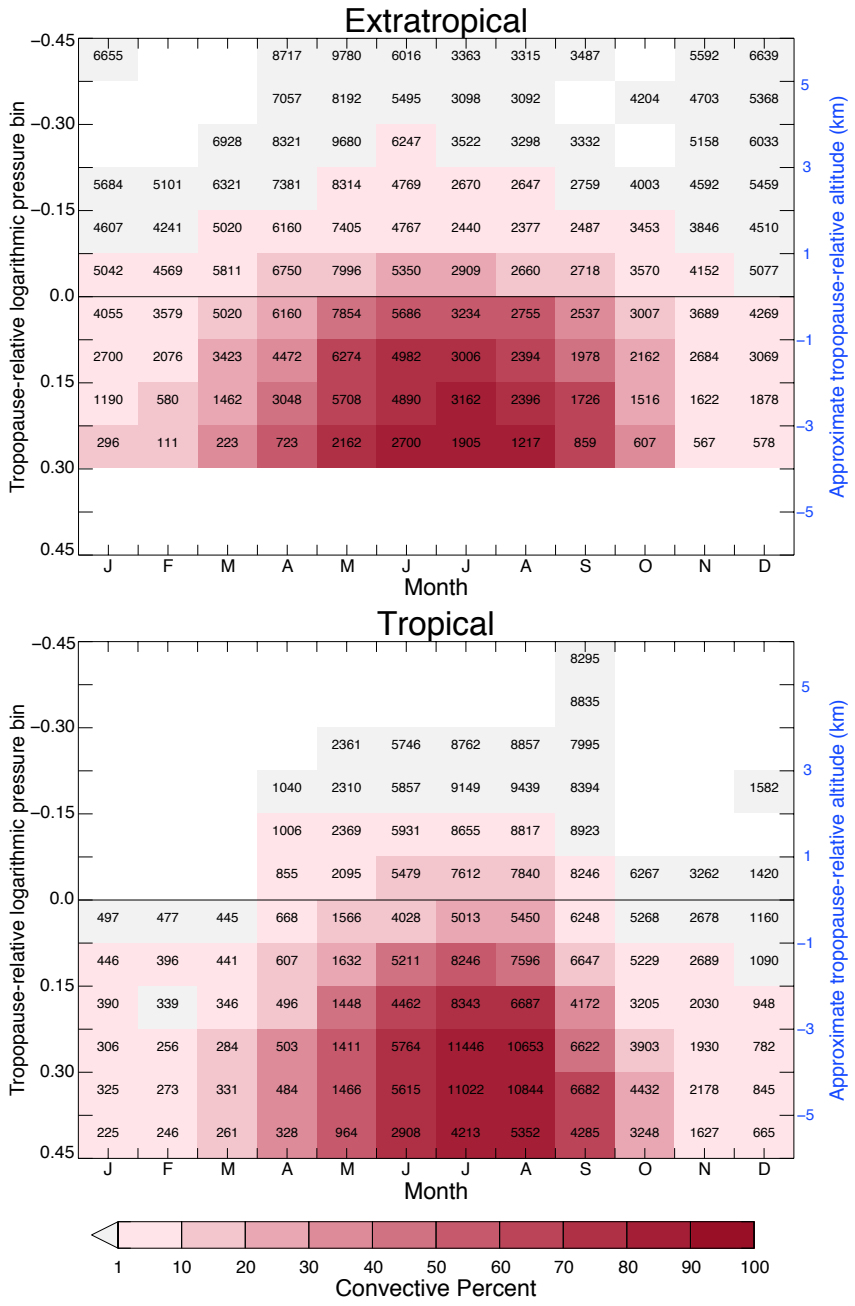

Figure 5.2: The percent of all trajectory-matched MLS layers associated with convection in each tropopause-relative logarithmic pressure bin for each month in (top) extratropical and (bottom) tropical environments. The solid line represents the tropopause. The numbers within each month-pressure box indicate the total number of matches (both convective and echo-free) in that tropopause-relative layer.

associated with convection as a function of tropopause-relative altitude for extratropical and tropical environments in Figure 5.2. There exists a clear seasonal cycle, with convective influence in the extratropical UT peaking from May-August with up to 50% of the immediate ∼1 km layer below the tropopause being recently impacted by convection. In the lowest ∼1 km of the stratosphere, up to 20% of trajectory-matched MLS layers were recently impacted by convection in April-September, and up to 30% in June and July. For tropical environments, UT convective influence peaks slightly later in the season with the most frequent occurrence in July and August (when such high-tropopause environments are most frequent over the CONUS). The frequency of convective influence near and above the tropopause in tropical environments is lower than in extratropical environments, occurring up to only 30% of the time in the first ∼1 km below the tropopause. This likely stems from the fact that the tropical tropopause is higher and convection does not reach these levels as often. However, convective influence on the LS is still prevalent in tropical environments, with up to 20% of trajectory-matched MLS layers in the first ∼1 km above tropopause being convectively influenced in June-August. Outside of these peak times, we see that convection is capable of impacting the composition of the UTLS throughout the entire year although the frequency is somewhat minimal. A growing body of work has additionally suggested that environments favorable for deep convection will become more frequent in the future as a result of anthropogenic climate change, thus increasing the overall influence of convection on the composition of the UTLS (e.g., Trapp et al., 2007; Gensini and Mote, 2015; Hoogewind et al., 2017).

Chapter 6

Conclusions and General Discussion

This study examined convection-driven changes in concentrations of H_2O, O_3, and CO in the UTLS using trajectory-matched radar observations of convection and satellite observations of composition. In particular, for a 13-year period, we matched ground-based weather radar observations across the CONUS (GridRad data) with downstream Aura MLS trace gas profiles using the TRAJ3D trajectory model. This allowed for the comparative analysis of convectively-influenced and non-influenced MLS profiles to quantify convective impact on UTLS composition. It was found that in extratropical and tropical environments (delineated by a tropopause pressure of 150 hPa), H_2O concentrations are substantially increased throughout the UTLS due to convection, as expected (Figs. 4.2a, 4.2b, 4.9a, 4.9b). In the extratropical LS, convective moistening is often between 10–100% with a median increase of ∼60% at an altitude of ∼1 km above the tropopause. Median H_2O increases in tropical environments range from 10–45% throughout the LS. Large increases ($\geq$ 100%) in the tropical LS occur less than 10% of the time, likely due to both low temperatures and high pre-convective relative humidity associated with the high tropopause in these environments (e.g., Schoeberl et al., 2019). Convection-driven reductions in O_3 in the LS were found in both extratropical and tropical environments, with a maximum decrease occurring two levels (∼2 km) above the tropopause at −24% and −34%, respectively (Figs. 4.3a, 4.3b, 4.10a, 4.10b). Lofting and mixing of low-O_3 tropospheric air into the LS is likely a large driver of the O_3 decrease, but the differences in the magnitude of the decrease between environments may be related to additional factors as discussed in Chapter 5. Extratropical and tropical concentrations of CO increase under convective influence, though exact changes are difficult to quantify due

to limited measurement precision and accuracy (Figs. 4.3c, 4.3d, 4.10c, 4.10d). There does appear to be a peak increase in CO concentration occurring two levels (∼3 km) below the tropopause in tropical environments, which may be indicative of the LMD of convection occurring in such environments.

Extratropical environments were also further classified based on the tropopause type (ST or DT) at the location of convection or trajectory initialization (Figs. 4.5, 4.6, 4.11, 4.12). This had little or no impact on H_2O concentration, which was somewhat unexpected given previous work showing that the presence of a DT can be related to deeper convective overshooting (Homeyer et al., 2014; Solomon et al., 2016). Alternatively, convection in DT environments did show larger increases in LS CO concentrations than in ST environments, which does suggest an increased efficiency of upward cross-tropopause transport in convection within DT environments. Furthermore, analyzing the fraction of trajectory matches associated with convection indicated that convection reaches the tropopause at similar rates in ST and DT environments, but reaches altitudes in the LS at higher rates in DT environments (Fig. 4.4). The extratropical tropopause type breakdown of O_3 concentrations revealed a much greater distinction between convective influence in ST and DT environments, with a ST pseudo-profile that can be characterized by convection-driven decreases in O_3 and a DT profile with little overall convective influence. This is likely related to the complex vertical distribution of O_3 in the UTLS when a DT is present (an "S"-shaped profile in the stratosphere). With convection-driven upward and downward cross-tropopause transport likely occurring within the UTLS, the impact on O_3 concentration from any particular storm is likely highly variable and dependent on the depth of overshooting. Thus, a wide range of increases and decreases in O_3 can be expected given both in-mixing of low-O_3 tropospheric air and vertical overturning of high and low O_3 layers within the background stratosphere. The analysis here

demonstrates that the end result is a near-zero median change in O_3 from convection in DT environments.

Using a simple, two-layer mixing model, we further investigated how convection-driven reductions of LS O_3 were greater in tropical environments than extratropical environments. We showed that the observed reductions of O_3 could not be acheived through mixing alone based on the observed echo-free O_3 concentrations. In fact, we showed that if mixing were equivalent in extratropical and tropical environments, approximately 10% of the observed 34% decrease in tropical environments would have to come from other sources. We speculate that, since our analyses show tropical environments commonly fall within the temperature-H_2O thresholds specified by Anderson et al. (2012, 2017) for chlorine activation to occur, the enhanced O_3-reduction found in tropical environments may be a result of chemical destruction.

The results presented here build upon a growing body of work on the influence of convection on UTLS composition, and more specifically, its impact on concentrations of H_2O, O_3, and CO. While it is generally agreed upon in prior work that midlatitude convection acts to moisten the UTLS, the extent to which it occurs has been debated. Although several studies have shown that convection transports copious H_2O into the LS in individual events, some work suggests that the overall role it plays is minor compared to larger-scale processes (e.g., Randel et al., 2015). Our results suggest that convection over the CONUS contributes substantially to LS H_2O during the warm season in both high and low tropopause environments, at least for short timescales of up to three days. In contrast to previous aircraft observations of convective influence in the UTLS, the finding of substantial O_3 and CO changes in the LS in this study is somewhat surprising. Given the order of magnitude and greater change in H_2O from UT to LS, its concentration (compared to the remaining trace gases examined here) is expected to be most sensitive to convective influence, followed by O_3 (about a factor of 4 change) and CO (a factor of $\sim$2). Following convection occurrence, mixing

of influenced air prior to downstream sampling by MLS will dilute any composition changes that take place, making it most difficult to assess O_3 and CO changes in these observations. Past aircraft observations have seldom shown large changes in trace gases such as O_3 and CO following convection, while H_2O changes vary broadly. There are some potential explanations for the difference between aircraft observations and our results. First, since aircraft observations of convective transport are uncommon, it is possible that the envelope of transport outcomes has not been well characterized by existing observations. Moreover, analysis of aircraft observations of gases other than H_2O in convective plumes has not been routinely documented in prior studies, leaving characterization of their changes largely unexplored. Second, due to the broad layers over which MLS retrieves trace gas observations, it is possible that changes in trace gases that are more confined to the UT or LS are distributed further across the tropopause in this analysis than in reality. There is a wide range in outcomes found here (and in recent modeling studies), so it is likely that these and other factors may be impacting the results.

While this study has contributed valuable insights, there are some limitations that hinder our ability to determine precise impacts of convection on the UTLS that can be improved upon in future work. First, both the spatial and temporal resolution of MLS observations are coarse with respect to the scales of convection. Currently, there are few high-resolution aircraft observations that have extensively sampled convectively influenced air in the LS (mostly limited to those recently collected during the Deep Convective Clouds and Chemistry [DC3] experiment and the Studies of Emissions, Atmospheric Composition, Clouds and Climate Coupling by Regional Surveys [SEAC^{4}RS] field campaign). Fortunately, an upcoming field campaign supported by NASA - Dynamics and Chemistry of the Summer Stratosphere (DCOTSS) - will provide a large dataset of high-resolution aircraft observations of

tropopause-overshooting convective influence on UTLS composition in the near future. Second, convective echo-top altitudes as observed by radar have an uncertainty of 1 km. Increased vertical resolution of radar observations would decrease this uncertainty, though current satellite-based alternatives pass at non-optimal times (0130 AM/PM LT) for observing convection. Additionally, the benefits of increased vertical resolution are likely minimal for trajectory-matching with MLS. Third, representations of the atmosphere are only provided every three hours by MERRA-2 and every six hours by ERA-Interim. It would be beneficial to use more reanalyses to ensure robustness of results across multiple datasets, and to increase wind field resolution to hourly which would in turn decrease horizontal displacement errors in the trajectories (Bowman et al., 2013). Finally, because our trajectory calculations are initialized in and outside of convection only within the CONUS and the history of the tracked air masses prior to their transit across the CONUS is unknown, it is possible that convective influence is substantially underestimated due to echo-free trajectories having recent convective origins outside of the CONUS and longer-term association with convection than that captured by our trajectories (e.g., hydration 10 days prior rather than 3 days prior). Such convective contamination of our echo-free population would be most likely during late summer, when deep (and often, tropopause-overshooting) convection has been occurring for long periods of time and can be found frequently nearby over the Sierra Madre Occidental of Mexico and in south-central Canada (e.g., Liu et al., 2020). Deep convection over the Sierra Madre is most frequent, but transit times of influenced air to the CONUS are often slow due to long paths followed initially west, then north and east through the North American upper troposphere monsoon anticyclone. Outflow from deep convection over Canada may be advected rapidly into the analysis domain, but such storms are much less common than those over the high Plains of the CONUS. In future work, backwards trajectories could also be calculated for initialized convective and echo-free particles. This would allow for

better and extended understanding of the history of convectively-influenced and non-influenced air, and allow for the analysis of pre-convective trace gas concentrations.

This study represents an important step in understanding the convective impact on UTLS composition. It is the first major co-utilization of the NEXRAD network of radar observations with MLS trace gas observations to examine composition changes in H_2O, O_3, and CO. We show that the trajectory-matching method reveals clear convective influences on these trace gases with unprecedented sampling. This signifies an important step in better characterizing radiative impacts of convection for representation in climate modeling. As the frequency and intensity of convection is likely sensitive to anthropogenic climate change, an understanding of these impacts could prove even more crucial in the future. Subsequent work with Aura MLS and alternative, higher-resolution satellite observations should be carried out to continue to characterize convective influence on UTLS composition and its variability. In particular, should a unique trace gas signature of convective influence be found, the global and long-term impacts of convection on UTLS composition could be assessed purely from a chemical perspective. Furthering our understanding of global convection-chemistry-climate linkages is vital as we work to improve representation of STE in climate model simulations.

Bibliography

Anderson, J. G., D. M. Wilmouth, J. B. Smith, and S. D. S, 2012: Uv dosage levels in summer: Increased risk of ozone loss from convectively injected water vapor. *Science*, **337**, 835–839, doi:10.1126/science.1222978.

Anderson, J. G., and Coauthors, 2017: Stratospheric ozone over the united states in summer linked to observations of convection and temperature via chlorine and bromine catalysis. *Proceedings of the National Academy of Sciences*, **114 (25)**, E4905–E4913, doi:10.1073/pnas.1619318114.

Bedka, K. M., J. Brunner, R. Dworak, W. Feltz, J. Otkin, and T. Greenwald, 2010: Objective satellite-based detection of overshooting tops using infrared window channel brightness temperature gradients. *Journal of Applied Meteorology and Climatology - J APPL METEOROL CLIMATOL*, **49**, 181–202, doi:10.1175/2009JAMC2286.1.

Bedka, K. M., and K. Khlopenkov, 2016: A probabilistic multispectral pattern recognition method for detection of overshooting cloud tops using passive satellite imager observations. *J. Appl. Meteor. Climatol.*, **55**, 1983–2005, doi:10.1175/JAMC-D-15-0249.1.

Berendes, T. A., J. R. Mecikalski, W. M. MacKenzie Jr., K. M. Bedka, and U. S. Nair, 2008: Convective cloud identification and classification in daytime satellite imagery using standard deviation limited adaptive clustering. *Journal of Geophysical Research: Atmospheres*, **113 (D20)**, doi:10.1029/2008JD010287.

Biondi, R., W. J. Randel, S.-P. Ho, T. Neubert, and S. Syndergaard, 2012: Thermal structure of intense convective clouds derived from gps radio occultations. *Atmospheric Chemistry and Physics*, **12 (12)**, 5309–5318, doi:10.5194/acp-12-5309-2012.

Boothe, A. C., and C. R. Homeyer, 2017: Global large-scale stratosphere–troposphere exchange in modern reanalyses. *Atmospheric Chemistry and Physics*, **17 (9)**, 5537–5559, doi:10.5194/acp-17-5537-2017.

Bowman, K. P., 1993: Large-scale isentropic mixing properties of the antarctic polar vortex from analyzed winds. *Journal of Geophysical Research: Atmospheres*, **98 (D12)**, 23 013–23 027, doi:10.1029/93JD02599.

Bowman, K. P., and G. D. Carrie, 2002: The mean-meridional transport circulation of the troposphere in an idealized gcm. *Journal of the Atmospheric Sciences*, **59 (9)**, 1502–1514, doi:10.1175/1520-0469(2002)059⟨1502:TMMTCO⟩2.0.CO;2.

Bowman, K. P., and C. R. Homeyer, 2017: GridRad - Three-Dimensional Gridded NEXRAD WSR-88D Radar Data. Research Data Archive at the National Center

for Atmospheric Research, Computational and Information Systems Laboratory, URL http://rda.ucar.edu/datasets/ds841.0/, doi:10.5065/D6NK3CR7.

Bowman, K. P., J. Lin, A. Stohl, R. Draxler, P. Konopka, A. Andrews, and D. Brunner, 2013: Input data requirements lagrangian trajectory models. *Bulletin of the American Meteorological Society*, **94**, 1051–1058, doi:10.1175/BAMS-D-12-00076.1.

Cooney, J. W., K. P. Bowman, C. R. Homeyer, and T. M. Fenske, 2018: Ten year analysis of tropopause-overshooting convection using gridrad data. *Journal of Geophysical Research: Atmospheres*, **123 (1)**, 329–343, doi:10.1002/2017JD027718.

Crum, T. D., and R. L. Alberty, 1993: The wsr-88d and the wsr-88d operational support facility. *Bull. Amer. Meteor. Soc.*, **74 (9)**, 1669–1688, doi:10.1175/1520-0477(1993)074⟨1669:TWATWO⟩2.0.CO;2.

Dee, D. P., and Coauthors, 2011: The era-interim reanalysis: configuration and performance of the data assimilation system. *Quarterly Journal of the Royal Meteorological Society*, **137 (656)**, 553–597, doi:10.1002/qj.828.

Dessler, A. E., and S. C. Sherwood, 2004: Effect of convection on the summertime extratropical lower stratosphere. *Journal of Geophysical Research: Atmospheres*, **109 (D23)**, doi:10.1029/2004JD005209.

Frey, W., and Coauthors, 2015: The impact of overshooting deep convection on local transport and mixing in the tropical upper troposphere/lower stratosphere (utls). *Atmospheric Chemistry and Physics*, **15 (11)**, 6467–6486, doi:10.5194/acp-15-6467-2015.

Fujita, T. T., 1974: Overshooting thunderheads observed from ats and learjet. Tech. Rep. NASA-CR-138595, University of Chicago, Department of Geophysical Sciences, Chicago, IL, United States.

Gelaro, R., and Coauthors, 2017: The Modern-Era Retrospective Analysis for Research and Applications, Version 2 (MERRA-2). *J. Clim.*, **30**, 5419–5454, doi:10.1175/JCLI-D-16-0758.1.

Gensini, V., and T. Mote, 2015: Downscaled estimates of late 21st century severe weather from ccsm3. *Climatic Change*, **129**, doi:10.1007/s10584-014-1320-z.

Gettelman, A., P. Hoor, L. L. Pan, W. J. Randel, M. I. Hegglin, and T. Birner, 2011: The extratropical upper troposphere and lower stratosphere. *Reviews of Geophysics*, **49 (3)**, doi:10.1029/2011RG000355.

Hanisco, T. F., and Coauthors, 2007: Observations of deep convective influence on stratospheric water vapor and its isotopic composition. *Geophysical Research Letters*, **34 (4)**, doi:10.1029/2006GL027899.

Hassim, M. E. E., and T. P. Lane, 2010: A model study on the influence of overshooting convection on TTL water vapour. *Atmos. Chem. Phys.*, **10**, 9833–9849, doi:10.5194/acp-10-9833-2010.

Hegglin, M. I., and Coauthors, 2004: Tracing troposphere-to-stratosphere transport above a mid-latitude deep convective system. *Atmospheric Chemistry and Physics*, **4 (3)**, 741–756, doi:10.5194/acp-4-741-2004.

Herman, R. L., and Coauthors, 2017: Enhanced stratospheric water vapor over the summertime continental United States and the role of overshooting convection. *Atmos. Chem. Phys.*, **17**, 6113–6124, doi:10.5194/acp-17-6113-2017.

Holton, J. R., P. H. Haynes, M. E. McIntyre, A. R. Douglass, R. B. Rood, and L. Pfister, 1995: Stratosphere-troposphere exchange. *Reviews of Geophysics*, **33 (4)**, 403–439, doi:10.1029/95RG02097.

Homeyer, C. R., 2014: Formation of the enhanced-v infrared cloud-top feature from high-resolution three-dimensional radar observations. *Journal of the Atmospheric Sciences*, **71 (1)**, 332–348, doi:10.1175/JAS-D-13-079.1.

Homeyer, C. R., 2015: Numerical simulations of extratropical tropopause-penetrating convection: Sensitivities to grid resolution. *J. Geophys. Res. Atmos.*, **120**, 7174–7188, doi:10.1002/2015JD023356.

Homeyer, C. R., and K. P. Bowman, 2013: Rossby wave breaking and transport between the tropics and extratropics above the subtropical jet. *Journal of the Atmospheric Sciences*, **70 (2)**, 607–626, doi:10.1175/JAS-D-12-0198.1.

Homeyer, C. R., and K. P. Bowman, 2017: Algorithm Description Document for Version 3.1 of the Three-Dimensional Gridded NEXRAD WSR-88D Radar (GridRad) Dataset. Available online at: http://gridrad.org/pdf/GridRad-v3.1-Algorithm-Description.pdf.

Homeyer, C. R., K. P. Bowman, and L. L. Pan, 2010: Extratropical tropopause transition layer characteristics from high-resolution sounding data. *J. Geophys. Res.*, **115**, D13 108, doi:10.1029/2009JD013664.

Homeyer, C. R., K. P. Bowman, L. L. Pan, E. L. Atlas, R.-S. Gao, and T. L. Campos, 2011: Dynamical and chemical characteristics of tropospheric intrusions observed during start08. *Journal of Geophysical Research: Atmospheres*, **116 (D6)**, doi:https://doi.org/10.1029/2010JD015098.

Homeyer, C. R., and M. R. Kumjian, 2015: Microphysical characteristics of overshooting convection from polarimetric radar observations. *J. Atmos. Sci.*, **72**, 870–891, doi:10.1175/JAS-D-13-0388.1.

Homeyer, C. R., and Coauthors, 2014: Convective transport of water vapor into the lower stratosphere observed during double-tropopause events. *Journal of Geophysical Research: Atmospheres*, **119 (18)**, 10,941–10,958, doi:10.1002/2014JD021485.

Hoogewind, K. A., M. E. Baldwin, and R. J. Trapp, 2017: The impact of climate change on hazardous convective weather in the united states: Insight from high-resolution dynamical downscaling. *Journal of Climate*, **30 (24)**, 10 081–10 100, doi:10.1175/JCLI-D-16-0885.1.

Jensen, E. J., A. S. Ackerman, and J. A. Smith, 2007: Can overshooting convection dehydrate the tropical tropopause layer? *Journal of Geophysical Research: Atmospheres*, **112 (D11)**, doi:10.1029/2006JD007943.

Jensen, E. J., and Coauthors, 2020: Assessment of observational evidence for direct convective hydration of the lower stratosphere. *Journal of Geophysical Research: Atmospheres*, **125 (15)**, e2020JD032 793, doi:10.1029/2020JD032793.

Jiang, J. H., N. J. Livesey, H. Su, L. Neary, J. C. McConnell, and N. A. D. Richards, 2007: Connecting surface emissions, convective uplifting, and long-range transport of carbon monoxide in the upper troposphere: New observations from the aura microwave limb sounder. *Geophysical Research Letters*, **34 (18)**, doi:10.1029/2007GL030638.

Lacis, A., D. Wuebbles, and J. Logan, 1990: Radiative forcing of climate by changes in the vertical distribution of ozone. *Journal of Geophysical Research: Atmospheres*, **95 (D7)**, 9971–9981, doi:10.1029/JD095iD07p09971.

Liu, C., and E. J. Zipser, 2005: Global distribution of convection penetrating the tropical tropopause. *Journal of Geophysical Research: Atmospheres*, **110 (D23)**, doi:10.1029/2005JD006063.

Liu, N., and C. Liu, 2016: Global distribution of deep convection reaching tropopause in 1year gpm observations. *Journal of Geophysical Research: Atmospheres*, **121 (8)**, 3824–3842, doi:10.1002/2015JD024430.

Liu, N., C. Liu, and L. Hayden, 2020: Climatology and detection of overshooting convection from 4 years of GPM precipitation radar and passive microwave observations. *J. Geophys. Res. Atmos.*, **125**, e2019JD032 003, doi:10.1029/2019JD032003.

Livesey, N. J., and Coauthors, 2020: Earth Observing System (EOS) Aura Microwave Limb Sounder (MLS): Version 4.2x Level 2 data quality and description document. Available online at: https://mls.jpl.nasa.gov/data/v4-2_data_quality_document.pdf.

Maddox, E. M., and G. L. Mullendore, 2018: Determination of best tropopause definition for convective transport studies. *Journal of the Atmospheric Sciences*, **75 (10)**, 3433–3446, doi:10.1175/JAS-D-18-0032.1.

Mullendore, G. L., A. J. Homann, K. Bevers, and C. Schumacher, 2009: Radar reflectivity as a proxy for convective mass transport. *Journal of Geophysical Research: Atmospheres*, **114 (D16)**, doi:10.1029/2008JD011431.

Pan, L. L., and L. A. Munchak, 2011: Relationship of cloud top to the tropopause and jet structure from calipso data. *Journal of Geophysical Research: Atmospheres*, **116 (D12)**, doi:10.1029/2010JD015462.

Pan, L. L., W. J. Randel, B. L. Gary, M. J. Mahoney, and E. J. Hintsa, 2004: Definitions and sharpness of the extratropical tropopause: A trace gas perspective. *Journal of Geophysical Research: Atmospheres*, **109 (D23)**, doi:10.1029/2004JD004982.

Pan, L. L., and Coauthors, 2009: Tropospheric intrusions associated with the secondary tropopause. *Journal of Geophysical Research: Atmospheres*, **114 (D10)**, doi:10.1029/2008JD011374.

Pan, L. L., and Coauthors, 2014: Thunderstorms enhance tropospheric ozone by wrapping and shedding stratospheric air. *Geophysical Research Letters*, **41 (22)**, 7785–7790, doi:10.1002/2014GL061921.

Phoenix, D. B., C. R. Homeyer, M. C. Barth, and S. B. Trier, 2020: Mechanisms responsible for stratosphere-to-troposphere transport around a mesoscale convective system anvil. *Journal of Geophysical Research: Atmospheres*, **125 (10)**, e2019JD032 016, doi:10.1029/2019JD032016.

Randel, W. J., E. Moyer, M. Park, E. Jensen, P. Bernath, K. Walker, and C. Boone, 2012: Global variations of hdo and hdo/h2o ratios in the upper troposphere and lower stratosphere derived from ace-fts satellite measurements. *Journal of Geophysical Research: Atmospheres*, **117 (D6)**, doi:10.1029/2011JD016632.

Randel, W. J., D. J. Seidel, and L. L. Pan, 2007: Observational characteristics of double tropopauses. *Journal of Geophysical Research: Atmospheres*, **112 (D7)**, doi:10.1029/2006JD007904.

Randel, W. J., K. Zhang, and R. Fu, 2015: What controls stratospheric water vapor in the nh summer monsoon regions? *Journal of Geophysical Research: Atmospheres*, **120 (15)**, 7988–8001, doi:10.1002/2015JD023622.

Robrecht, S., and Coauthors, 2019: Mechanism of ozone loss under enhanced water vapour conditions in the mid-latitude lower stratosphere in summer. *Atmos. Chem. Phys.*, **19**, 5805–5833, doi:10.5194/acp-19-5805-2019.

Schoeberl, M. R., E. J. Jensen, L. Pfister, R. Ueyama, M. Avery, and A. E. Dessler, 2018: Convective hydration of the upper troposphere and lower stratosphere. *Journal of Geophysical Research: Atmospheres*, **123 (9)**, 4583–4593, doi:10.1029/2018JD028286.

Schoeberl, M. R., L. Pfister, T. Wang, J. Kummer, A. E. Dessler, and W. Yu, 2020: Erythemal radiation, column ozone, and the north american monsoon. *Journal of Geophysical Research: Atmospheres*, **125 (13)**, e2019JD032 283, doi:10.1029/2019JD032283, e2019JD032283 2019JD032283.

Schoeberl, M. R., and Coauthors, 2019: Water vapor, clouds, and saturation in the tropical tropopause layer. *Journal of Geophysical Research: Atmospheres*, **124 (7)**, 3984–4003, doi:10.1029/2018JD029849.

Schwartz, M. J., G. L. Manney, M. I. Hegglin, N. J. Livesey, M. L. Santee, and W. H. Daffer, 2015: Climatology and variability of trace gases in extratropical double-tropopause regions from mls, hirdls, and ace-fts measurements. *Journal of Geophysical Research: Atmospheres*, **120 (2)**, 843–867, doi:10.1002/2014JD021964.

Schwartz, M. J., W. G. Read, M. L. Santee, N. J. Livesey, L. Froidevaux, A. Lambert, and G. L. Manney, 2013: Convectively injected water vapor in the north american summer lowermost stratosphere. *Geophysical Research Letters*, **40 (10)**, 2316–2321, doi:10.1002/grl.50421.

Smith, J. B., and Coauthors, 2017: A case study of convectively sourced water vapor observed in the overworld stratosphere over the united states. *Journal of Geophysical Research: Atmospheres*, **122 (17)**, 9529–9554, doi:10.1002/2017JD026831.

Solomon, D. L., K. P. Bowman, and C. R. Homeyer, 2016: Tropopause-penetrating convection from three-dimensional gridded nexrad data. *Journal of Applied Meteorology and Climatology*, **55 (2)**, 465–478, doi:10.1175/JAMC-D-15-0190.1.

Solomon, S., K. H. Rosenlof, R. W. Portmann, J. S. Daniell, S. M. Davis, T. J. Sanford, and G.-K. Plattner, 2010: Contributions of stratospheric water vapor to decadal changes in the rate of global warming. *Science*, **327 (5970)**, 1219–1223, doi:10.1126/science.1182488.

Starzec, M., G. L. Mullendore, and C. R. Homeyer, 2020: Retrievals of convective detrainment heights using ground-based radar observations. *Journal of Geophysical Research: Atmospheres*, **125 (5)**, e2019JD031 164, doi:10.1029/2019JD031164.

Stohl, A., G. Wotawa, P. Seibert, and H. Kromp-Kolb, 1995: Interpolation errors in wind fields as a function of spatial and temporal resolution and their impact on different types of kinematic trajectories. *Journal of Applied Meteorology (1988-2005)*, **34 (10)**, 2149–2165, doi:10.1175/1520-0450(1995)034⟨2149:IEIWFA⟩2.0.CO;2.

Tilmes, S., and Coauthors, 2010: An aircraft-based upper troposphere lower stratosphere o3, co, and h2o climatology for the northern hemisphere. *Journal of Geophysical Research: Atmospheres*, **115 (D14)**, doi:10.1029/2009JD012731.

Trapp, R. J., N. S. Diffenbaugh, H. E. Brooks, M. E. Baldwin, E. D. Robinson, and J. S. Pal, 2007: Changes in severe thunderstorm environment frequency during

the 21st century caused by anthropogenically enhanced global radiative forcing. *Proceedings of the National Academy of Sciences of the United States of America*, **104 (50)**, 19 719–19 723, doi:10.1073/pnas.0705494104.

Ueyama, R., E. J. Jensen, and L. Pfister, 2018: Convective influence on the humidity and clouds in the tropical tropopause layer during boreal summer. *Journal of Geophysical Research: Atmospheres*, **123 (14)**, 7576–7593, doi:10.1029/2018JD028674.

Waters, J. W., and Coauthors, 2006: The earth observing system microwave limb sounder (eos mls) on the aura satellite. *IEEE Transactions on Geoscience and Remote Sensing*, **44 (5)**, 1075–1092.

World Meteorological Organization, 1957: *A three-dimensional science: Second session of the commission for aerology*.

Xian, T., and C. R. Homeyer, 2019: Global tropopause altitudes in radiosondes and reanalyses. *Atmospheric Chemistry and Physics*, **19 (8)**, 5661–5678, doi:10.5194/acp-19-5661-2019.